Archaeol Anthropol Sci (2018) 10:41–60
DOI 10.1007/s12520-016-0339-7

ORIGINAL PAPER

Luminescence geochronology and paleoenvironmental implications of coastal deposits of southeast Cyprus

Evangelos Tsakalos[1,2] · Constantin Athanassas[1] · Polychronis Tsipas[3] · Maria Triantaphyllou[4] · Maria Geraga[2] · George Papatheodorou[2] · Eleni Filippaki[1] · John Christodoulakis[1] · Maria Kazantzaki[1]

Received: 18 September 2015 / Accepted: 25 April 2016 / Published online: 11 May 2016
© Springer-Verlag Berlin Heidelberg 2016

Abstract Quaternary stratigraphy and sea level changes have been extensively investigated in many areas of the Mediterranean. However, numerical dating of coastal deposits and the associated paleoenvironmental information are limited for the coasts of Cyprus, principally based on radiometric and radiation-exposure geochronological techniques on fossils which bear a range of limitations and uncertainties. As such, optically stimulated luminescence (OSL) dating techniques are deemed to be the most suitable in direct dating of the coastal sediments of Cyprus. In the southeastern Cyprus, coastal dunes (aeolianites) now forming elongated ridges appear as morphological features running parallel to the current shoreline presenting an indicator of sea level and climate changes of great paleoenvironmental significance. We present our first chronological results for the exposed aeolianites and underlying littoral deposits formed along the southeastern coastal Cyprus ranging from 78.4 ± 9.9 to 56.2 ± 7.4 ka. The post-infrared–infrared stimulated luminescence (pIR-IRSL) revealed that dune formation took place during the marine isotope stages (MISs) 3, 4, and possibly 5a. Late Holocene reworking is proposed for a distinctively isolated dune with an age of ~1.3 ka ago. This study also showed that pIR-IRSL dating of feldspars may be a reliable alternative to quartz OSL dating when the quartz luminescence characteristics are unsuitable.

Keywords Cyprus paleoenvironment · Sea level change · Coastal deposits · Luminescence dating · IRSL

✉ Evangelos Tsakalos
e.tsakalos@inn.demokritos.gr

[1] Laboratory of Archaeometry, Institute of Nanoscience and Nanotechnology, National Centre for Scientific Research, N.C.S.R. "Demokritos", 15310 Athens, Greece

[2] Laboratory of Marine Geology and Physical Oceanography, Department of Geology, University of Patras, 26504 Rio, Greece

[3] Laboratory of Molecular Beam Epitaxy (MBE), Institute for Nanoscience and Nanotechnology, National Centre for Scientific Research, N.C.S.R. "Demokritos", 15310 Athens, Greece

[4] Faculty of Geology and Geoenvironment, Department of Historical Geology-Palaeontology, University of Athens, Panepistimiopolis, 15784 Athens, Greece

Introduction

Cyprus occupies a strategic position in untangling sea level changes in the Eastern Mediterranean as well as in resolving the neotectonic and paleoenvironmental evolution of the northern Levant in the Quaternary.

Following major secular oceanic sea level trends in response to Quaternary polar ice buildup and decay (e.g., Imbrie et al. 1984; Lea et al. 2002; Shackleton et al. 1984; Shackleton 1987), recurring Pleistocene and Holocene sea level fluctuations in the Eastern Mediterranean (e.g., Lambeck 1996; Lambeck and Purcell 2005; Pavlopoulos et al. 2006; Pirazzoli 2005; Vouvalidis et al. 2005) have produced a range of coastal landforms and sedimentary sequences on the uplifting shores of Cyprus, which are expressed as raised marine terraces and beachrocks draped by backshore dune calcarenites (Bagnall 1960; Kinnaird 2008; Moseley 1976; Pantazis 1967; Turner 1971a; Poole 1992; Poole and Robertson 1991, 1998; Tsiolakis and Zomeni 2008; Zomeni 2012). Over and above, Cyprus's position at the doorstep of the arid landscapes of Anatolia and the Syro-Palestine that is a key in regional paleoenvironmental reconstructions as sedimentological, paleontological, and occasionally paleoanthropological indicators

(Ammerman et al. 2006, 2008) could potentially reflect on the paleoenvironmental qualities of the island and the neighboring areas during the geologically recent past. For instance, archaeological recent studies have revealed human presence on several coastal sites of the island, with Akrotiri Aetokremmos, Nissi Beach, and Akamas Aspros being dated to the late Epipaleolithic (ca. 11,000–10,000 cal BC) (Ammerman 2010; Knapp 2010) and considered as the oldest evidence for seagoing in the Eastern Mediterranean.

Several studies have used dating methods to establish the time framework of aeolianites and beachrock formation and assess their connection with sea level changes (e.g., Bateman et al. 2004; Jacobs et al. 2003, 2006; Mauz et al. 2009, 2012, 2013). These studies have demonstrated that the time of formation of the major aeolian deposits around the world is similar at several locations (Brooke 2001). However, there are cases where deposition during Quaternary has varied between regions.

Aeolianites are mainly thought to be deposited around the world at sea level highstands (e.g., Hearty and Kindler 1997; Murray-Wallace et al. 1998, 2010). However, there is some evidence indicating that dune formation has also taken place during the Last Glacial (Engelmann et al. 2001; Frechen et al. 2001; Kendrick et al. 1991; Porat and Wintle 1995; Price et al. 2001) at lowered sea level.

Furthermore, there are instances where last interglacial aeolianites are not matched in thickness and spatial distribution by comparable Holocene aeolianites (e.g., Woodroffe et al. 1995). Differences in the timing of deposition and morphology of aeolian dunes during major sea level changes (highstands, lowstands) among regions appear to be dependent on the interactions caused by minor-secondary sea level changes, local climatic conditions, sediment availability, and differences in the inland-near-shore topography (e.g., Vacher et al. 1995).

Correlation of aeolian deposits among the East Mediterranean and the establishment of a common time framework for their development, linking climatic events to paleosea levels, should be made with great caution. In the Mediterranean, aeolianites are common features mainly appearing as topographic heights sitting on middle to late Quaternary marine terraces. In the coastal Mallorca region in Spain for instance, carbonate dunes have been dated as marine isotope stages (MISs) 10 and 8 (Nielsen et al. 2004). Other chronological studies in the region of Baleares Islands of Mallorca (Fornós et al. 2009; Hillaire-Marcel et al. 1996) have also pointed out that aeolian and marine units were deposited during high sea levels of isotope stage 5.

In the Eastern Mediterranean, sand dunes have been mainly studied along the coasts of Israel and Lebanon. On northern Israel, shallow marine and dune units composed of quartz and bioclastic grains shape a Pleistocene sequence up to 40 m thick (Sivan and Porat 2004). Sivan and Porat (2004) have assigned the Carmel (northern coastal plain of Israel) coastal deposits within the late Pleistocene, during several episodes in the time interval of ~100–35 ka, a period of dramatically changing sea levels. Furthermore, early studies on aeolianites rich in quartz and feldspars, found in the central coast of Israel, have assigned the development of the aeolian dunes during an interglacial age, from oxygen isotope stage 5 to 11 (Gavish and Friedman 1969). Lately however, luminescence dating results of feldspars in the area (Engelmann et al. 2001; Frechen et al. 2001, 2002; Porat and Wintle 1995; Porat et al. 2004) disagree with the previous study and suggest that the four aeolian ridges near Netanya and Tel Aviv were deposited during the last 65 ka, mainly during the oxygen isotope stages 3 and 4 at a lower sea level than previously suggested. Particularly, Porat et al. (2004) applied a single-aliquot additive dose (SAAD) infrared stimulated luminescence (IRSL) protocol and found that units of the western kurkar ridge had an age of <65 ka, which confirmed the previous multiple-aliquot additive dose (MAAD) IRSL and thermoluminescence (TL) age estimates (Engelmann et al. 2001; Frechen et al. 2002).

On the north coastal Egypt, studies using a variety of chronological methods (U/Th, ^{14}C, AAR, electron spin resonance (ESR), and optically stimulated luminescence (OSL)) on coastal ridges made of beach, paleosol, and aeolianite deposits have revealed ages ranging from Holocene for the ridge nearest to the coast, followed by a last interglacial and an oxygen isotope stage 7 dune unit as moving toward the inner ridges (El-Asmar 1994; El-Asmar and Wood 2000).

Moving to the west, on the Tunisian coast, Paskoff and Sanlaville (1986) assigned two dune formations to the late Pleistocene, which sit on a last interglacial beach unit. Additionally, OSL ages of aeolianites obtained in a study in Cap Bon peninsula (northeastern Tunisia) (Elmejdoub et al. 2011) revealed ages clustering around the last interglacial period (125–75 ka), implying that the former stratigraphic allocation of these dunes (Oueslati 1994; Paskoff and Sanlaville 1983) was inaccurate. Further, sand dune systems in Sardinia have been dated as MIS 5 (Pascucci et al. 2014; Thiel et al. 2010; Andreucci et al. 2010), while Mauz et al. (1997) reported TL results for the northwest coast of Sicily with ages suggesting a MIS 5e deposition. A luminescence dating study was conducted in the Calabrian coast of southern Italy; coastal deposits were also dated at the last interglacial (Balescu et al. 1997).

Our knowledge however on the chronological framework of coastal deposits in the coasts of the Aegean is limited. Early studies on sedimentary deposits found on raised marine terraces along the coasts of Crete have revealed the existence of characteristic Pleistocene marine fauna (e.g., *Strombus bubonius*, *Patella safina*, *Conus testudinarius*) (Boekschoten 1963; Dermitzakis 1973; Dermitzakis and De Vos 1986; Hogrel 1974; Kelletat 1979; Mercier et al. 1974; Mourtzas 1990; Moutzas and Fytrolakis 1988; Peters 1985; Psarianos

1961; Symeonides 1967). Furthermore, U/Th dating has also confirmed the existence of a late Pleistocene age for the sediments found on the lower terraces with ages suggesting a MIS 5 deposition for the south and a MIS 4 for the north coastal areas of Crete (Angelier 1979).

More recently, in a TL dating study (Polymeris et al. 2012) of aeolianites in the coasts of Tenedos (Bozcaada) Island, in North Aegean Sea, ages revealed that deposition and cementation of these sediments took place between the early stage of MIS 2 and the very late phase of MIS 3. Furthermore, Athanassas and Zacharias (2010) provided a chronological framework for raised marine sequences in the southwest coast of Greece during the Upper Quaternary, by employing recuperated-OSL (re-OSL) dating. An aeolianite sample was dated 68 ± 9 ka which corresponds to MIS 4. Lately, Athanassas et al. (2012) explored the paleogeographic conditions at two Paleolithic sites found on a fossilized dune field in the coastal plain of Navarino in southwest Greece. The aeolianites on the site were dated to a MIS 3 period.

The necessity to quantify geodynamic and earth-surface processes in the coastal sectors of Cyprus had been acknowledged by several authors since long time (e.g., Birot and De Vaumas 1962). However, it was no earlier than the 1990s when researchers came to apply numeric dating to Quaternary coastal deposits of Cyprus (Poole 1992; Schellmann and Kelletat 2001; Schellmann et al. 2008) and lately Zomeni (2012) by employing well-established techniques such as uranium-series (Th/U) and ESR dating on molluscan fauna incorporated in the deposits themselves. Despite the maturity of radiometric and radiation-exposure geochronological techniques in fossil dating, there have been circumstances where chronologies based on the fossil content were questioned (e.g., Goy et al. 2003). As such, OSL dating techniques are deemed to be more promising in direct dating of the coastal sediments of Cyprus.

Despite the plenty of quartz found in the coastal deposits of Cyprus, data shown later indicate that quartz's OSL signals are insensitive and affected by unstable underlying components, resulting in highly scattered paleodose estimates. Difficulties induced in dating by problematic luminescence behavior of quartz can be overcome by employing IRSL of feldspar (Steffen et al. 2009).

Recent efforts have facilitated the use of feldspars in the luminescence dating of Quaternary sediments. Specifically, the "post-infrared infrared stimulated luminescence," known as pIRIR, retains all benefits of feldspar dating, such as intense signals under laboratory stimulation and considerably higher saturation levels, and additionally deals with the problem of anomalous fading (Spooner 1994; Wintle 1973). The pIRIR procedure is based on elevated temperature IRSL stimulations on feldspars carried out immediately after conventional 50 °C IR readings, giving rise to signals with lower fading rates (Thomsen et al. 2008). Particularly, fading rates associated to pIRIR signals at 290 °C ($pIRIR_{290}$) are negligible (Thiel et al. 2010; Thomsen et al. 2011). On this background, the single-aliquot regenerated ($pIRIR_{290}$-SAR) procedure introduced by Thiel et al. (2011a) is now widely applied (Buylaert et al. 2011, 2012; Lowick et al. 2012; Roskosch et al. 2012; Schatz et al. 2012; Stevens et al. 2011; Thiel et al. 2011a, b, 2012; Vasiliniuc et al. 2012).

The purpose of this paper is to reexamine the chronology of coastal deposits of southeast Cyprus by employing up-to-date luminescence methods to wit the pIRIR signals at 290 °C from feldspar. In this work, special focus is given to the deposits of the southeast coast, between Ayia Napa and Cape Greco (Fig. 1). New radiometric ages from the same sites have recently been published (Zomeni 2012). In this regard, available radiometric ages put additional strain on the effectiveness of $pIRIR_{290}$ dating, as independent age control on the latter remains scarce in literature to date.

Description of sample sites and sampled outcrops

The formations that concern our work comprise the youngest members of the Cenozoic "circum-Troodos sedimentary succession" that envelopes the ultramafic basement of Troodos mountains (Fig. 1 and Table 1).

They consist of coastal deposits arranged in a more or less monotonous stratigraphy, as seen from the coastal cliffs, that stretches all along the south coast of Cyprus (Fig. 2), shallow marine to beach sediments covered by calcite-cemented aeolian sediments, with the latter dominating in both thickness and spatial extent (Poole 1992).

Numerous sites along the Cypriot coastal sequence have been the subject of former geochronological studies. In the earliest of these works (e.g., Birot and De Vaumas 1962; Ducloz 1964, 1968; Horowitz 1965; Moshkovitz 1963; Pantazis 1966a, b, c, 1967; Turner 1971a, b), discovery of characteristic fauna (e.g., *Strombus bubonious*) indicated a late interglacial age for these deposits. Initial assessments were further backed by subsequent radiometric and relative dating (Galili et al. 2009, 2011; Noller 2009; Poole 1992; Schellmann and Kelletat 2001; Schellmann et al. 2008; Theodorou 2005; Zomeni 2012) in most cases, confirming the findings of the former studies which were based on paleontological observations (Table 1).

Many published absolute ages for the coastal sediment succession of Cyprus seem to cluster around the following two distinct Quaternary stages: the last and the penultimate interglacial, meaning the MIS 5 and 7, respectively. MIS 5 littoral sediments have been ascertained for the entire south coast, almost uninterruptedly from Cape Greco to the east through Paphos to Akamas to the west, while MIS 7 sites are fewer, mainly outcropping at Larnaca, Petounda, Coral Bay, and Cape Geronisos (Galili et al. 2009, 2011; Poole 1992;

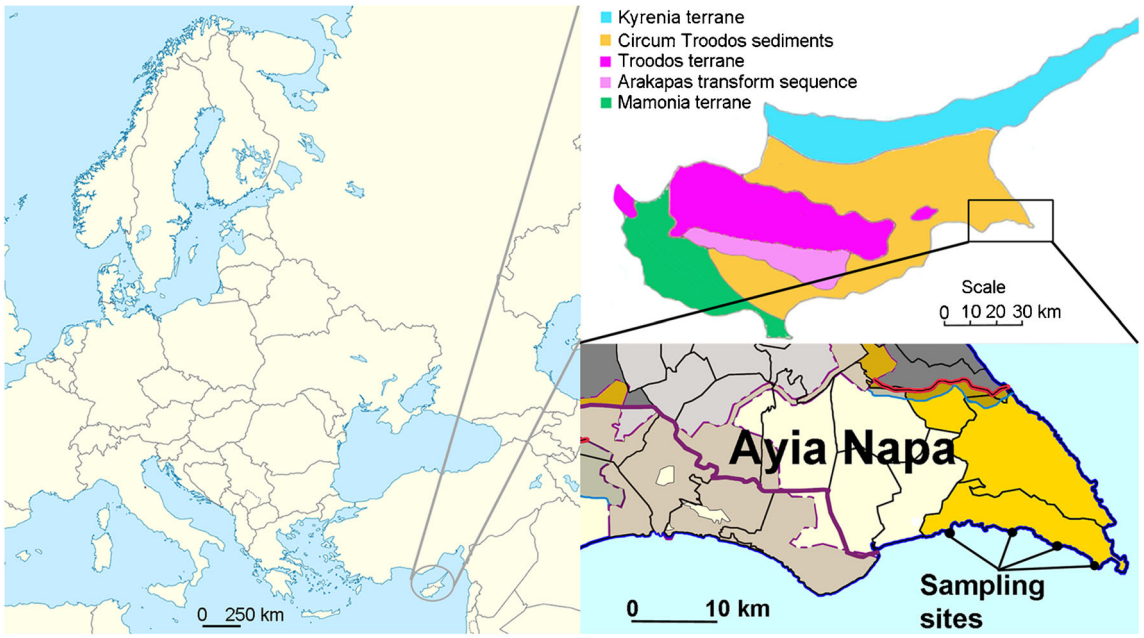

Fig. 1 Study area and sampling site of the studied aeolianites and littoral deposits

Schellmann and Kelletat 2001; Schellmann et al. 2008; Theodorou 2005). There are cases however where U/Th results on *Cladocora caespitosa* are assigned to MIS 6 (Poole et al. 1990; Zomeni 2012). Marine deposits of both MISs 5 and 7 occur at elevations ranging from 5 to 15 m asl approximately, and this variability is attributed to differential uplift owing to faults activating between sites. Of particular significance to our study are two published aeolianite OSL ages from Ayia Napa (Noller 2009), which indicated that aeolinites formation took place during the MISs 3 and 4.

The aeolianites and the underlying marine sediments that are preserved at Cape Greco and the greater area of Ayia Napa are investigated in this study (Fig. 1). The aeolianites form a hummocky relief above erosion surfaces, more commonly appearing as individual topographic highs or backing up over paleocliffs. The aeolianites, which run parallel to the coast, have their crest right at the current coastline (Fig. 3). The upper top of the dunes contain pillar-like structures, namely, rhizoliths (McLaren 1995; Mount and Cohen 1984) with evident morphological micrite tube features (calcified root systems) formed through the interaction of root-induced organic and inorganic processes (Klappa 1980).

The depositional character of the coastal sandstones encountered in the study area presupposed sufficient exposure to daylight prior to deposition, and for this reason, both the aeolianites and the shallow marine sediments are most suitable for luminescence analysis. Due to the cemented nature of the deposits, sampling involved extraction of rectangular blocks from spots of interest (seen in Fig. 1). Altogether, nine samples were taken for luminescence dating (seven aeolianites and two littoral deposits).

Luminescence dating

Sample preparation and measurement facilities

Following conventional laboratory practices (e.g., Preusser et al. 2008), quartz and feldspar coarse grains were prepared using the procedure of chemical treatment with 10 % hydrochloric acid to remove carbonate cements and 10 % hydrogen peroxide to remove organic content, drying, and sieving. Fractions were treated with hydrofluoric acid (40 and 10 % for quartz and feldspar, respectively) to avoid contribution of the alpha-irradiated outer part of the mineral, followed by a rinse with 10 % HCl (to remove fluorosilicate by-products), and a final sieving to separate traces of any remnant by-products. Purified quartz (treated with 40 % hydrofluoric acid for 90 min to remove all other minerals) and feldspar (heavy liquid separation) fractions mainly fell in the range of 80–125 μm. Single-aliquot measurements consisted of a monolayer of quartz or feldspar grains mounted on stainless steel disks of 10 mm diameter using silicone oil as an adhesive. Grains covered the central 5-mm-diameter portion of each disk, corresponding to several hundred grains per aliquot.

Measurements were carried out on a Risø TL-DA 15 luminescence reader fitted with a Thorn EMI photomultiplier tube. Irradiation was from a calibrated $^{90}Sr/^{90}Y$ β source. For feldspar, stimulation was by infrared light diodes emitting at 870 nm at 90 % power and detecting the luminescence signal in the blue-violet region (320–460 nm) with a Schott BG39/Corning 7–59 filter combination (known as filter pack). Infrared light stimulation was at 290 °C, right after a 50 °C stimulation for 100 s, which has shown insignificant

Table 1 Radiometric and relative dating of Quaternary coastal deposits of Cyprus

Location	Dating method	Material dated	Elevation (asl in meters)	Numerical or relative age (years BP)	Error (years BP)	Reference
Cape Greco	U/Th	*Cladocora caespitosa*	8	141,000	4,000	Poole (1992)
Cape Greco	U/Th	*Cladocora caespitosa*	8	219,000	16,000	Poole (1992)
Agia Napa	U/Th	*Cladocora caespitosa*	Not reported	143,400	9,300	Zomeni (2012)
Agia Napa	U/Th	*Cladocora caespitosa*	Not reported	152,000	7,600	Zomeni (2012)
Cape Greco	ESR	*Glycymeris* sp.	9.5	134,000	10,000	Schellmann and Kelletat (2001); Schellmann et al. (2008)
Cape Greco	ESR	*Glycymeris* sp.	9	137,000	24,000	Schellmann and Kelletat (2001); Schellmann et al. (2008)
Cape Greco	ESR	*Glycymeris* sp.	3.5	153,000	15,000	Schellmann and Kelletat (2001); Schellmann et al. (2008)
Cape Greco	ESR	*Glycymeris* sp.	3	130,000	14,000	Schellmann and Kelletat (2001); Schellmann et al. (2008)
Cape Greco	ESR	*Glycymeris* sp.	3	157,000	19,000	Schellmann and Kelletat (2001); Schellmann et al. (2008)
Cape Greco	ESR	*Glycymeris* sp.	3	204,000	22,000	Schellmann and Kelletat (2001); Schellmann et al. (2008)
Cape Greco	ESR	*Helix* sp. in *aeolianite*	14.5	72,000	5,000	Schellmann and Kelletat (2001); Schellmann et al. (2008)
Cape Greco	ESR	*Helix* sp. in *aeolianite*	14.5	67,000	6,000	Schellmann and Kelletat (2001); Schellmann et al. (2008)
Cape Greco	ESR	*Helix* sp. in *aeolianite*	11.5	88,000	10,000	Schellmann and Kelletat (2001); Schellmann et al. (2008)
Cape Greco	ESR	*Helix* sp. in *aeolianite*	11.5	66,000	4,000	Schellmann and Kelletat (2001); Schellmann et al. (2008)
Cape Greco	ESR	*Helix* sp. in *aeolianite*	11	70,000	7,000	Schellmann and Kelletat (2001); Schellmann et al. (2008)
Cape Greco	ESR	*Helix* sp. in *aeolianite*	11	71,000	6,000	Schellmann and Kelletat (2001); Schellmann et al. (2008)
Cape Greco	ESR	*Helix* sp. in *aeolianite*	12	6800	Not reported	Schellmann and Kelletat (2001); Schellmann et al. (2008)
Agia Napa	ESR	*Helix* sp. in *aeolianite*	12	84,000	6,000	Schellmann and Kelletat (2001); Schellmann et al. (2008)
Agia Napa	ESR	*Helix* sp. in *aeolianite*	12	95,000	7,000	Schellmann and Kelletat (2001); Schellmann et al. (2008)
Agia Napa	OSL	*aeolianite*	6	60,900	4,400	Noller (2009)
Agia Napa	OSL	*aeolianite*	16	57,900	5,200	Noller (2009)
Cape Greco	Paleontology	*Strombus bubonius* LMK	Not reported	125,000	Not reported	Theodorou (2005)
Cape Greco	Paleontology	*Strombus bubonius* LMK	Not reported	125,000	Not reported	Theodorou (2005)
Cape Greco	Paleontology	*Strombus bubonius* LMK	Not reported	125,000	Not reported	Theodorou (2005)
Keryneia	Paleontology	*Strombus bubonius* LMK	15–17	125,000	Not reported	Galili et al. (2009, 2011)

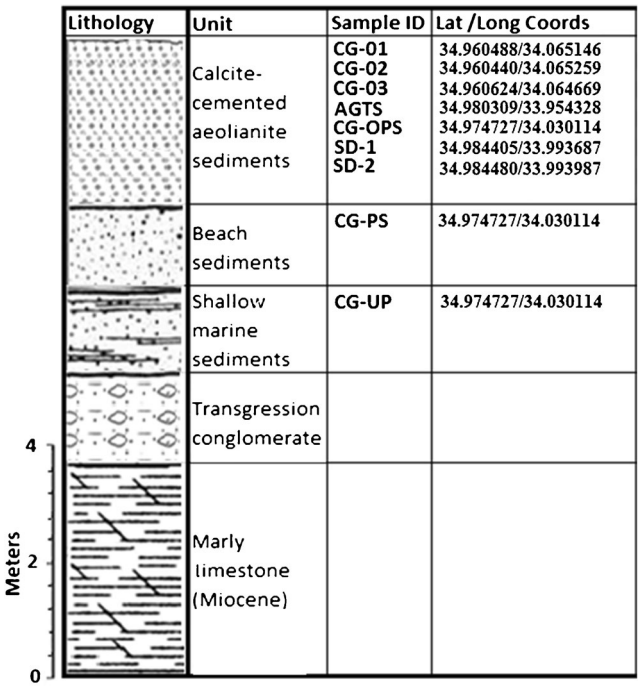

Fig. 2 A typical schematic composite stratigraphic column exposed in cliffs along SE Cyprus. Samples collected for luminescence dating are shown next to the column (CG-01, CG-02, etc)

anomalous fading (Thiel et al. 2011b). For two aeolian samples which gave young ages (~1.3 ka), infrared light stimulation was at 225 °C right after 50 °C, ensuring non-fading and minimum residual signal (Thiel et al. 2011b).

For quartz OSL, blue LEDs (470 nm) were used for stimulating the aliquots and a 7.5-mm Hoya U-340 filter was the signal detection filter mounted in front of the photomultiplier tube. The single-aliquot regenerative-dose (SAR) protocol after Murray and Wintle (2003) was applied for D_e measurements of quartz.

Dose rate determination

Dose rate relevant elements of the nine samples were determined individually. The calculation of the dose rates (U, Th, K) was based on analytical data obtained by inductively coupled plasma mass spectrometry (ICP-MS; ACME Laboratories, Canada). After chemical treatment to isolate K-feldspar, a scanning electron microscope (SEM) coupled with energy dispersive spectrometer (EDS) was used to confirm that the grains derived are indeed K-feldspar. For the nine samples, internal dose rates were also determined using both ICP-MS. Internal and external dose rates were calculated using the "The Dose Rate calculator (DRc)" software developed by Tsakalos et al. (2015). DRc uses the conversion factors proposed by Guérin et al. (2011) and the attenuation factors (due to water content) for alpha radiation by Aitken (1985), beta by Nathan and Mauz (2008), and gamma by Guérin and Mercier (2012). DRc also calculates the cosmic ray contribution to the total dose rate according to Prescott and Stephan (1982) and Prescott and Hutton (1988, 1994)) using the altitude and latitude of the sampling sites, present-day depth, and the density of the overburden. Water contents (%) were based on "as-found" values with an error of ±5 % and considered to remain constant during burial. The calculated dose rates are listed in Table 2. The final dose rates are obtained by correcting for etching of the grains and the grain size. To avoid potential problems related to an inhomogeneous gamma radiation field, samples were taken from thick lithological homogeneous sediment layers and far from lithological boundaries.

Additionally, in situ measurements were also carried out at all sampling spots using a calibrated handheld "*Saphymo-SRAT S.P.P.2 NF γ Scintillometer*" to test the reliability of the calculated gamma dose rate. SRAT is based on a 50-cm^3 sodium iodine scintillation detector enabling measuring of both cosmic and gamma radiations and allowing very high sensitivity (accuracy ±10 %). The SRAT's unit of measurement is counts per second (cps). The operation range for gamma radiation is 0.02 to 30 microsieverts per hour (μSv/h), convertible to Gy/ka using conversion factors.

Readings were obtained in 4π geometry, by placing the scintillator probe into the spots/hasms from which samples for luminescence dating were taken (10 repeated measurements for each spot, 100 s per reading). Systematic measurements were also performed at intervals of ~30 cm, covering a distance of at least 2 m from each sampling spot. However, assuring 4π geometry in each measurement, particularly when dealing with solidified and hard carbonaceous sediments, is

Fig. 3 **a** Typical appearance of the aeolianite formation in the sampling site of Cape Greco. **b** A close-up of the surface of the aeolianites

Table 2 Samples codes, radioelement contents, and other parameters utilized in dose rate calculations

Sample ID	U (ppm)		Th (ppm)		K (wt%)		Water (wt%)	Elevation (m)	Depth (cm)	Dose rate (Gy/ka)					
											ICP-MS			Scintillation	
	Extrinsic	Intrinsic	Extrinsic	Intrinsic	Extrinsic	Intrinsic				Cosmic	α	β	γ	γ	Total
CG-01	1.5	0.5	0.4	2.5	0.06	11	4.5 ± 0.23	18	30	0.27	0.29	0.68	0.19	0.19	1.44 ± 0.1
CG-02	1.1	0.4	0.5	1	0.06	10.5	4.3 ± 0.22	18	10	0.27	0.17	0.61	0.15	0.16	1.2 ± 0.1
CG-03	1.2	0.5	0.5	1.2	0.05	10.4	5.1 ± 0.26	12	20	0.27	0.21	0.61	0.16	0.16	1.25 ± 0.1
AGTS	1.3	0.2	0.5	0.7	0.06	9.8	4 ± 0.2	10	15	0.27	0.11	0.60	0.18	0.17	1.15 ± 0.1
CG-OPS	1.2	0.4	0.6	1.2	0.09	10.1	5.2 ± 0.26	17	10	0.27	0.19	0.63	0.17	0.17	1.25 ± 0.1
CG-PS	1.2	0.4	1.7	1.2	0.41	10.4	5.6 ± 0.28	16	100	0.16	0.19	0.89	0.30	0.30	1.54 ± 0.1
CG-UP	2.2	0.5	0.2	2.1	0.06	11	4.3 ± 0.22	15	200	0.14	0.28	0.76	0.26	0.27	1.43 ± 0.1
SD-1	2.3	0.9	0.9	3	1.04	10.5	3.6 ± 0.18	18	60	0.27	0.43	1.72	0.54	0.55	2.955 ± 0.2
SD-2	2.3	0.9	1	3	1.04	10.5	3.8 ± 0.19	18	10	0.27	0.43	1.72	0.54	0.55	2.96 ± 0.2

not always easy. In such cases, when 4π geometry cannot be confirmed, uncertainties are introduced. Nevertheless, ICP-MS analysis on the bulk sediment confirmed that 4π geometry was achieved as gamma dose rates derived using both ICP-MS and in situ measurements are in fair agreement; thus, extra confidence on the reliability of the derived dose rates is introduced.

It should be noted that the assessment of the dose rate for our samples is based on the infinite matrix assumptions (Aitken 1985; Roesch and Attix 1968). However, their relevance is only applicable to specific cases, mainly when the studied geological formation (in our case aeolianites being the predominating sediment) is homogeneous, the radiation is distributed uniformly, and there is material surrounding the dated mineral comparable to the range of the radiations (Nathan and Mauz 2008). Further, the state of (dis)equilibrium was not explored in this study, assuming radioactive equilibrium in the uranium decay series. Possible disequilibrium of uranium would have an effect on the calculated dose rate, something that has been documented in many studies (e.g., Krbetschek et al. 1994; Olley et al. 1996). However, the use of alkali feldspar grains will partially compensate for the uncertainties associated with disequilibrium of uranium and its effect on the total dose rate. The significant contribution of internal potassium to the total dose rate minimizes the effect of the possible disequilibrium of uranium in the calculation of the external dose rate (Li et al. 2008). Further, disequilibrium seems to be no critical in our study, since U concentrations of bulk sediment are systematically very low (in most cases between 1.1 and 1.5 ppm). Furthermore, in situ scintillometer measurements revealed (a) low natural radioactivity which is expected for the carbonaceous formations (aeolianites), (b) uniformly distributed radiation, and (c) absence of any factor that might cause disturbance in the natural radiation homogeneity (e.g., stratigraphic detachment, volcanic body intrusion, faulting or relevant tectonic unsettlement).

The grain size is 80–125 μm for all samples, except for SD-1 and SD-2, for which it is 125–200 μm

Luminescence measurements

Quartz OSL

When measuring quartz samples from the sample sites, it was revealed that OSL ages were unexpectedly low, greatly deviating from the expected paleoenvironmental framework, and highly scattered, even though the standard validation tests (preheat, bleaching, and dose recovery tests) were in most cases successful. Such age inconsistencies are sometimes interpreted as the result of differential bleaching of the quartz grains (Godfrey-Smith et al. 1988). Bailey et al. (2003) made use of the decay rate difference by plotting the equivalent dose (D_e) against stimulation time (D_e (t) plot) to examine incomplete bleached samples. A D_e (t) plot of a fully bleached sample should reveal a steady value of D_e with increasing stimulation time, while a rising D_e should be the case of an incompletely bleached sample. For our samples here, the D_e (t) plots showed a falling value of D_e with increasing integration time (Fig. 4), which has been interpreted (Bailey 2003; Bailey et al. 2003; Li and Li 2006; Rittenour et al. 2005; Shen and Mauz 2009) as being the consequence of thermal instability of one of the medium or slow OSL components. Therefore, for our samples concerned here, we concluded that differential bleaching is not the cause of such inconsistencies, but it is actually an uncommon behavior (thermal instability) of the signal components that gives inaccurate results.

In most cases, to obtain the D_e value using the SAR protocol, the bulk initial signal (e.g., the first 0.5 s) of the decay curve is integrated. The fast component which is usually dominant in the initial bulk signal (e.g., Jain et al. 2003) sometimes appeared to be weak. In such cases, the medium or the slow components of the decay curve may contribute significantly to the initial bulk signal, commonly leading to problematic D_e values. Particularly, erroneous D_e values have been observed when the ratio between the fast and medium components changes through the course of the SAR protocol, something that has been attributed to thermal instability or recuperation of the medium/slow components (Jain et al. 2003; Li and Li 2006).

Deconvolution of the continuous wave (CW)-OSL signals can further confirm such problematic cases (Bailey et al. 1997; Bulur et al. 2000; Choi et al. 2003; Jain et al. 2003; Murray and Wintle 2003). This can be done by fitting the CW-OSL curve to the three components of the decay curve (McKeever and Chen 1997, pp. 653). Figure 5 depicts the different proportions that each of the three components takes in the bulk signal from sample CG-OPS.

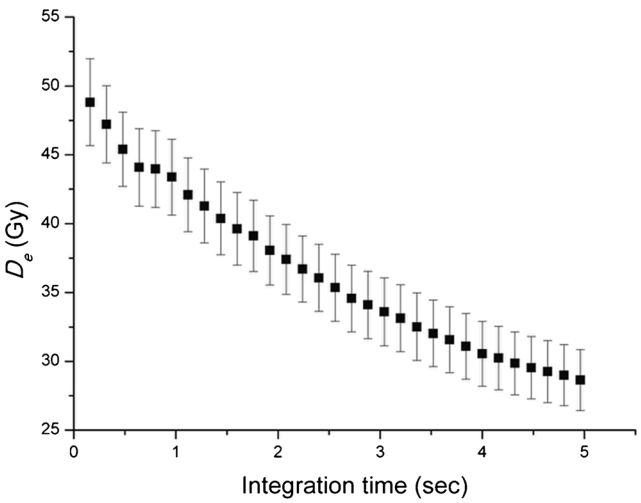

Fig. 4 D_e (t) plot for the natural signal of sample CG-OPS. Stimulation was by *blue* diode (470 ± 30 nm) at 90 % power. The D_e values were measured at successive intervals of 0.16 s. D_e (t) plot shows a continuous decrease of D_e with increasing integration time

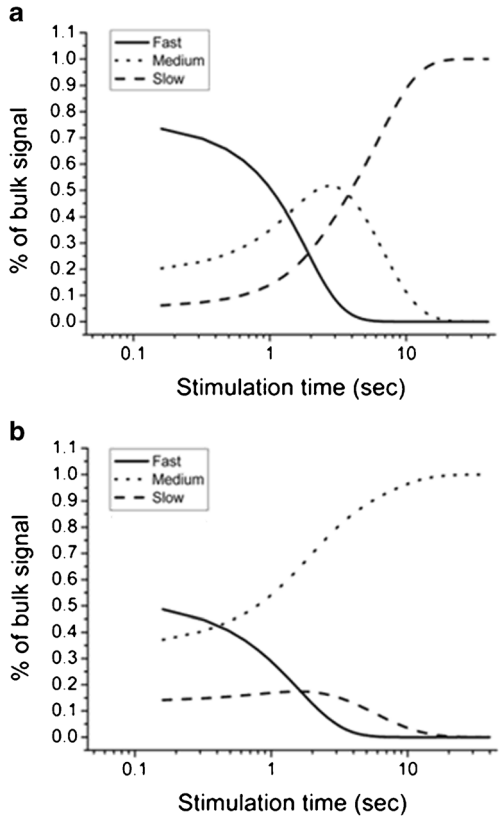

Fig. 5 Deconvoluted CW-OSL signal of CG-OPS sample. **a** Contribution of the components in natural bulk signal and **b** in the bulk-regenerated signal (after 108.78-Gy beta irradiation)

The "double-SAR" ("post-IR blue") protocol outlined by Roberts and Wintle (2001) and Banerjee et al. (2001) with a preheat at 240 °C for 10 s, and a cutheat at 160 °C for 10 s, was used for D_e determination.

It is easily observed that the fast component dominates the natural OSL signal (Fig. 5a), while in the subsequent regenerated dose (Fig. 5b), its relative contribution is comparable to a very strong medium component, something that is probably due to the thermal instability of the medium component (Li and Li 2006; Shen and Mauz 2009; Steffen et al. 2009), which is not observed in the natural signal as it has been faded through time. The derived D_e value calculated from the bulk initial signal would therefore be underestimated as a result of thermally unstable components underlying the initial bulk signal. We therefore decided to use feldspar grains to obtain D_e values that could be used to estimate accurate ages.

IRSL measurements

Single-aliquot equivalent dose measurements were derived using the post-IR IRSL (pIRIR) protocol after Thiel et al. (2011a) shown schematically in Table 3. For two samples which gave very young ages, we used a modified pIRIR protocol (Buylaert et al. 2009; Schmidt et al. 2011) which has been found to minimize the effect of anomalous fading and residual dose for young samples. This protocol measures a conventional IRSL signal at 50 °C ($IRSL_{50}$) and subsequently a pIRIR signal at 225 °C.

Table 3 pIRIR SAR protocol for coarse-grained feldspar measurements (after Thiel et al. 2011a)

Step	Treatment
1	Give dose
2	Preheat, 60 s at 320 °C
3	IR stimulation, 100 s at 50 °C
4	IR stimulation, 100 s at 290 °C
5	Give test dose
6	Cutheat, 60 s at 320 °C
7	IR stimulation, 100 s at 50 °C
8	IR stimulation, 100 s at 290 °C
9	IR stimulation, 40 s at 325 °C
10	Return to step 1

D_e values of the pIRIR signal at 290 and 225 °C were derived by integrating the signal of the initial 2 s from the decay curve, after subtracting the last 20 s as a background and fit the produced growth curves with an exponential plus linear term. The dose-response curve and the decay curve of one aliquot for $IRSL_{50}$ and $pIRIR_{290}$ are shown in Fig. 6a, b. The curves are representative for all the other samples measured. It is clear from Fig. 6 that stimulation at 50 °C gives rise to a natural IRSL signal that is weaker than the natural post-IRIR signal at 290 °C, by about 80 %. For $pIRIR_{290}$, Lx/Tx is well fitted to an exponential plus linear term. The $IRSL_{50}$ does not fit to an exponential plus linear term; thus, linear fitting was used for the representation of this signal. Recycling ratios for this aliquot were 0.93 ± 0.01 for the $IRSL_{50}$ and 1.03 ± 0.02 for $pIRIR_{290}$. Recuperation is absent at both stimulation temperatures, as no signal is detected at the zero (0) dose.

For both $pIRIR_{290}$ and $pIRIR_{225}$ signals, equivalent doses (D_e values) were chosen for further analysis if they had (i) recycling ratios within 10 % of unity and (ii) thermal transfer <3 % of the natural signal. Collectively, these selection criteria led to the exclusion of <10 % of the total measured aliquots.

Preheat tests As shown in the steps of the SAR protocol (Table 3), a high temperature is applied before the IRSL measurement (step 2 in Table 3). This is necessary so that electrons accumulated in any thermally unstable traps will be thermally stimulated and released, preventing their unwanted contribution to the stable IRSL signal that will be measured after. If an unwanted signal contributes to the IRSL signal, that would result in an increased D_e and therefore in a wrong overestimated age. In the "preheat test," a number of D_e values are determined using different temperatures which are plotted

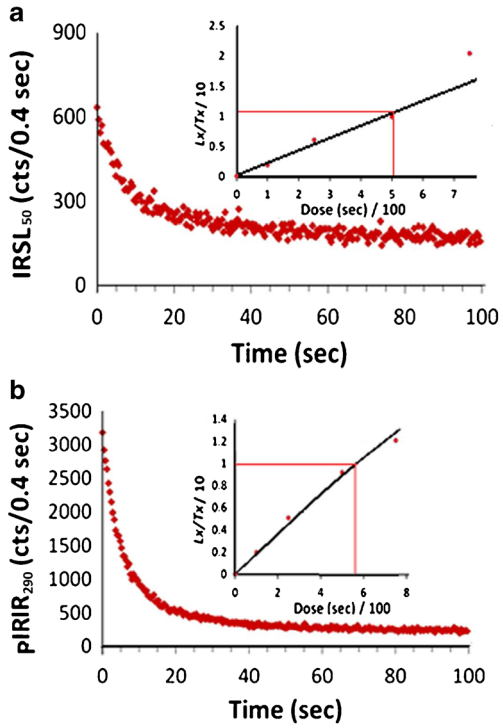

Fig. 6 Decay and dose-response curves for an aliquot of sample CG-OPS showing the $IRSL_{50}$ (**a**) and $pIRIR_{290}$ (**b**) signals from coarse-grained (80–125-μm) feldspars

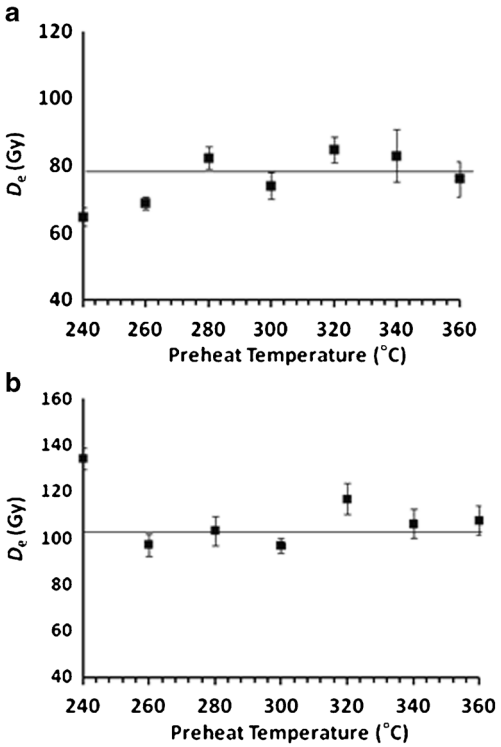

Fig. 7 **a** D_e as a function of preheat temperature for CG-OPS (aeolianite) and **b** CG-UP (shallow marine) samples. Aliquots were measured in groups of three (*squares* show means) using seven different preheat temperatures from 240 up to 360 °C (held for 60 s each). Six regeneration cycles were measured using the following doses for beta irradiation: 0, 34.4, 68.7, 114.5, 171.8, 0, and 34.4 Gy (test dose 11.5 Gy). The results were checked for sensitivity changes

against preheat temperatures (Murray and Olley 1999; Murray and Wintle 2000; Roberts et al. 1999). The preheat temperature which is taken for measurement should be in a plateau.

An appropriate preheat temperature of 320 °C was used after a preheat plateau test had been carried out on two samples (Fig. 7a, b). The test showed that D_e values become relatively stable at temperatures above 300 °C.

Bleachability of $pIRIR_{290}$ by natural light To test for sufficient signal resetting at the time of deposition, a bleaching test was performed. Studies have shown that signal zeroing in feldspar grains is slower compared to that of quartz (e.g., Godfrey-Smith et al. 1988; Klasen et al. 2006) which can contribute to the retention of some residual signal in the measurements, leading to an overestimation of the true age. Sixteen aliquots of sample CG-OPS were measured in groups of four having first been exposed at different times to sunlight. After 90 min of sun exposure, the sample retained ~3 Gy as residual for $pIRIR_{290}$ signal, which is in general ~4 % of the D_e value (73.2 Gy) of the sample as seen below (Fig. 8a, b).

Dose recovery To test the applicability of the pIRIR protocol using a stimulation temperature of 290 °C, the dose recovery test was applied (Murray and Wintle 2003). In the absence of independent dating, a dose recovery experiment could be used to examine where the SAR protocol can obtain the correct equivalent dose. Normally, the natural signal of the sample is zeroed with sunlight or in solar stimulator and then irradiated in the lab with a dose close to the natural D_e. Then, the given dose is measured using the SAR protocol to test if it can be recovered as a D_e. For a well-performing SAR protocol, the ratio between the given and measured dose should be close to unity (Murray and Wintle 2003), at least in the range between 0.9 and 1.1.

Six aliquots of CG-OPS sample were bleached by sun exposure for 6 h and then given a 80.15-Gy dose. The SAR protocol was then applied to test if the 80.15 Gy could be recovered.

The test showed that recovery ratios were within the 2σ level (0.9–1.1; Fig. 9a, b). The mean ratio ($N = 6$) of the given dose to recovered D_e was 0.96 ± 0.03, signifying that the SAR protocol generates a good D_e accuracy and precision. The average by the central age model (Galbraith et al. 1999) was 81.1 ± 2 (after residual subtraction), again within the 2σ level of the given dose of 80.15 Gy, indicating that the applied protocol is working as it should. Furthermore, all "recycling ratio" values for the same aliquots were within 5 % of unity (mean ratio 0.96 ± 0.05). We are thus confident that D_e estimates derived by the $pIRIR_{290}$-SAR protocol are accurately calculated.

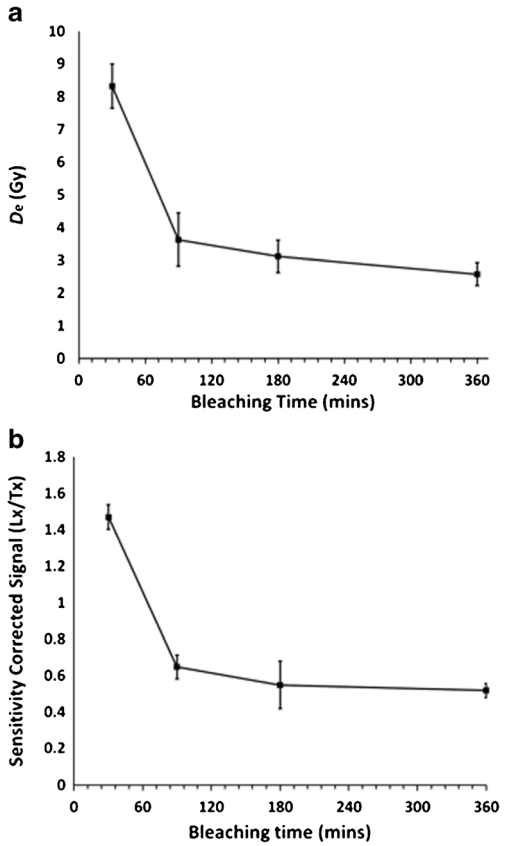

Fig. 8 Results of solar bleaching of the $pIRIR_{290}$ signal of sample CG-OPS for **a** D_e and **b** sensitivity-corrected signal shown as a function of bleaching time

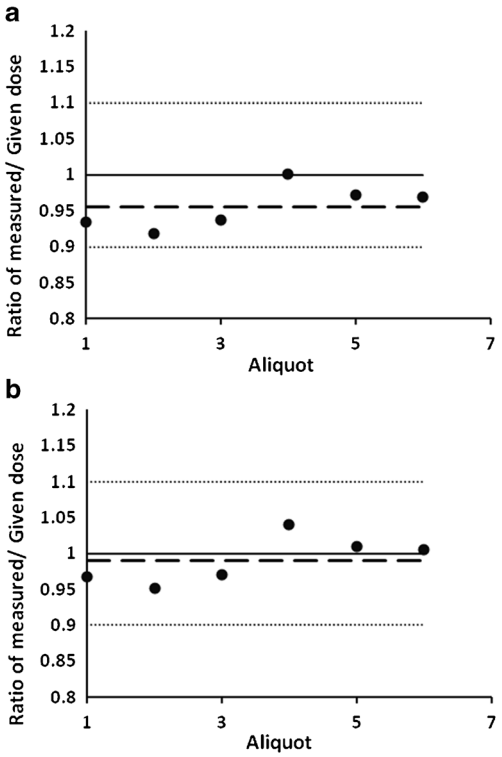

Fig. 9 Dose recovery test for CG-OPS sample **a** without residual subtraction and **b** with residual subtraction. *Black dots* indicate the measured/given ratio calculated for each aliquot. The target value is unity (*black line*). *Dashed line* shows the mean. The range of acceptability is between 0.9 and 1.1 (*dotted lines*)

Fading rate assessment Laboratory experiments have provided evidence that electrons from deep traps in feldspars are less stable than in quartz, something that is attributed to the tunneling of electrons out of otherwise stable traps. This means that there is a loss of the luminescence signal (Wintle 1973). It is therefore necessary to determine the rate of signal loss and then apply some forms of mathematical correction.

Different methods have been proposed to measure the loss of luminescence per decade of time (g value) (e.g., Auclair et al. 2003; Huntley and Lamothe 2001). In this study, the method developed by Huntley and Lamothe (2001) was applied, in which bleached aliquots are given a dose once and are short shined following increasing time delays.

The pIRIR protocol of Thiel et al. (2011a) described in "IRSL measurements" section above (Table 3) was used to determine the g values for the pIRIR at 290 °C using one aliquot for each sample. The g value of each aliquot was obtained by fitting a linear regression line to the sensitivity-corrected pIRIR signals as a function of logarithmic normalized elapsed time. For the $pIRIR_{290}$ signal, results obtained (Fig. 10) yield a mean g value of −2.34 % (considered as zero) with a standard deviation of ca. ±0.4 %, signifying that using this protocol, feldspar experiences no loss of signal (mean recuperation was 0.8 %).

Determination of the equivalent dose (D_e)

The establishment of the SAR protocol has revealed that different aliquots of the same sample give different equivalent doses. This has brought up the matter of how an equivalent dose distribution of a sample is to be depicted in order to get a meaningful and reliable representation and thus extract the necessary information for age calculations. A simple way of getting a first impression of how the equivalent doses of a sample are distributed is to produce a probability density function (PDF) (Fig. 11). However, the influence that an individual D_e value has upon the overall distribution cannot be seen and examined in a single probability density function.

To avoid the uncertainty inherent in PDFs, Galbraith et al. (1999) developed the "radial plot" for the presentation of single-aliquot data. Aliquots of a sample are depicted in a radial plot in Fig. 12. Here, the equivalent dose of each aliquot is displayed along with its associated measured uncertainty.

The variety in D_e distributions can indicate that a sample has been subjected to diverse bleaching conditions (Arnold et al. 2007; Olley et al. 1999; Rodnight et al. 2006) and post-depositional processes and/or millimeter-scale differences in the beta dose rate to individual grains (Jacobs and Roberts 2007) or even intrinsic differences in the luminescence sensitivity of the aliquots measured.

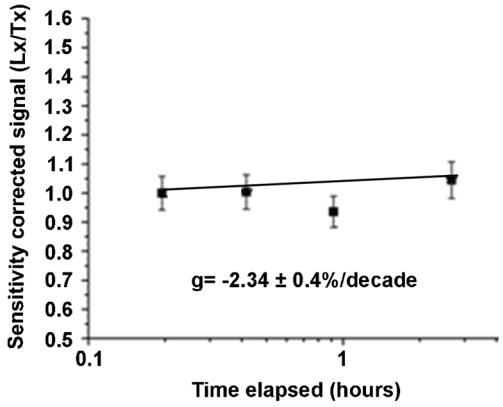

Fig. 10 Measurements of the mean g value for CG-OPS sample. The normalized $pIRIR_{290}$ intensities are plotted against the log of time elapsed since the end of the irradiation. The g value corresponds to the percentage fading loss per decade of time, hence to the slope of the weighted linear regression. A dose of 114.5 Gy was given

A number of different methodologies are available that can assist in obtaining the best estimate of D_e (e.g., Lepper and McKeever 2002; Olley et al. 1998; Stokes et al. 2001), and of these, the most widely used are those of Galbraith et al. (1999). Many studies have used overdispersion values as the only diagnostic criterion for the choice of the most appropriate methodology (e.g., Olley et al. 2004a). This value gives an estimate of the relative standard deviation of the true D_e values, remaining after the measurement error of each aliquot has been taken into account; if the measurement error was the only reason for the variation observed in D_e, then the overdispersion would be zero. For well-bleached and homogeneous aeolianites, an overdispersion value close to zero would be expected.

However, in a study testing the accuracy of various statistical models, Bailey and Arnold (2006) concluded that the selection of the most appropriate age model based only on a single descriptor for the D_e distribution (such as the degree of overdispersion) is not possible, and that no single method of analysis is applicable to all samples (depositional environments), and proposed that the decision process should include a series of criteria which describe the shape of the equivalent

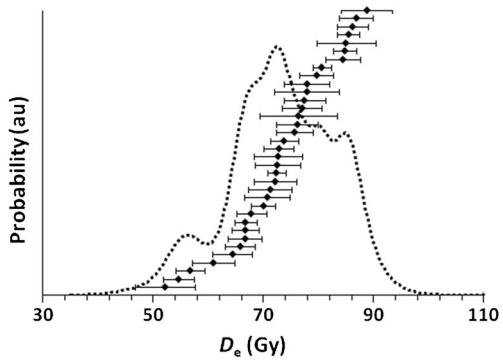

Fig. 11 Probability density function of CG-OPS (*dotted line*). The individual D_e values (shown with associated errors as *bars*) are plotted in rank order

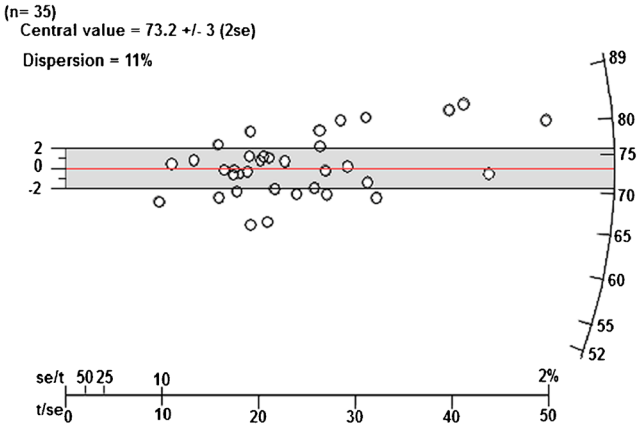

Fig. 12 Radial plot for CG-OPS sample. The *shaded area* represents the values that fall within two standard deviations of the weighted mean (an equivalent dose value of 73.2 Gy). D_e values are shown together with their associated precision. Values plotted on the *left* are those measured with low precision, while moving to the *right*, precision is higher. An additional feature of great interest in radial plots is that a radial line drawn from the origin passes through points that have equal D_e values but different precision. Data points that fall outside the two standard deviations of the weighted mean can be used to determine the degree of overdispersion (e.g., 0 % overdispersion means that 95 % of all dose estimates lie within ±2 standard deviations of a "common true value" (Galbraith et al. 1999; Galbraith and Roberts 2012), in this case ±2 standard deviations of the weighted mean). In this instance, the data are overdispersed by 11 %

dose distribution (skewness, kurtosis, overdispersion, and the presence of negative D_e values). Bailey and Arnold (2006) also developed a decision process guide (Bailey and Arnold 2006, pp. 2500) that can be used to help choose the most suitable model on a case-by-case basis.

In our study, the D_e distributions of the measured aliquots show some scatter with values of skewness ranging from 0.1 to 1.4 and kurtosis 0.1 to 3.1. The overdispersion values ranged between 4 and 20 %. Based on these suggestions, the central age model (CAM) by Galbraith et al. (1999) was used for eight samples which show tight distributions approaching normality (Table 4) and low scatter (skewness, kurtosis, and overdispersion). For the D_e distribution of sample CG-02 which exhibits a broader spread, we applied the minimum age model (MAM) to determine the appropriate D_e value. The CAM calculates the weighted mean taking into account additional dispersion that comes from measurement uncertainties (Galbraith et al. 1999). The MAM can be used for heterogeneous bleached samples and identifies the well-bleached aliquots by applying a truncated normal distribution to the log D_e values (Galbraith and Laslett 1993; Galbraith et al. 1999). The width of this minimum D_e population is derived from statistical measurement errors of each D_e value and the overdispersion.

Table 4 contains the descriptive statistics which facilitated the age model decision procedures based on Bailey and Arnold (2006) and the range of pIRIR D_e values derived. Table 4 also compares the D_e values derived using the CAM

Table 4 Determination of the most likely equivalent dose using numerical parameters

Sample	D_e distribution characteristics			D_e (Gy)		Model selection	
	Overdispersion	Skewness	Kurtosis	Mean	Weighted mean[a]	Model	D_e (Gy)
CG-OPS	11 %	−0.4	−0.1	73.4 ± 9.2	73.5 ± 1.7	CAM	73.2 ± 1.5
CG-UP	17 %	−0.1	−1.6	118.9 ± 22.7	116.4 ± 8.6	CAM	116.8 ± 6.1
CG-PS	20 %	0.5	−0.9	97.7 ± 20.3	94.9 ± 6.5	CAM	95.9 ± 5.2
CG-01	19 %	−0.3	−0.2	94 ± 18.2	93.4 ± 8	CAM	92.4 ± 5.2
CG-02	16 %	1.4	3.1	86.7 ± 15.3	84.5 ± 6.1	MAM	86.9 ± 7.5
CG-03	21 %	0.6	0.6	99 ± 21.7	94.8 ± 8.1	CAM	96.9 ± 5.8
AGTS	9 %	0.1	−1.5	80.3 ± 7.8	78.2 ± 2.6	CAM	79.8 ± 2.2
SD-01	4 %	0.7	1.4	4.1 ± 0.5	3.9 ± 0.2	CAM	3.9 ± 0.1
SD-02	18 %	0.8	1.6	3.9 ± 0.9	3.8 ± 0.3	CAM	3.9 ± 0.3

[a] For the weighted mean, each value was weighted by $1/\sigma D_e$

and MAM with the mean and the weighted mean. Data indicates that skewness, kurtosis, and overdispersion values do not greatly affect feldspar dose distributions, as the dose estimates using the two age models do not differ significantly compared to mean and weighted mean. However, using the age models, the associated D_e errors are reduced considerably compared with the mean D_e errors.

Scattered D_e values as a result of incomplete/diverse bleaching of the luminescence signal is mainly a concern for sediments that have been exposed to sunlight only for a short period of time such as fluvial deposits (Arnold et al. 2007, 2009; Olley et al. 1999). However, many studies have shown samples that had been well bleached (aeolian deposits) at the time of burial, experiencing significant spread and overdispersion (e.g., up to 20 %) in their equivalent dose values (e.g., Jacobs et al. 2003; Olley et al. 2004b; Roberts et al. 2000). Duller (2008) argued that this overdispersion is the additional scatter in the data that cannot be explained by the calculated uncertainties, most probably the result of a combination of remaining intrinsic factors that cannot be suitably accounted for (e.g., Thomsen et al. 2003) and extrinsic factors such as microdosimetry. Close proximity of feldspar grains to radioactive heavy minerals, such as zircons, would contribute to a higher beta dose (Roberts et al. 1999). Dark-colored minerals (indicative of some heavy minerals) were found after chemical treatment in many of the samples used in this study.

Based on the successful recovery of the artificially induced dose (dose recovery test) and taking into account that the samples were deposited under conditions which allowed for sufficient and uniform signal resetting, we suppose that the reasons for the slightly scattered dose distributions observed are based predominantly on post-depositional processes (grains displaced by groundwater percolation and by small-scale activities of fauna) and millimeter-scale differences in the beta dose rate to individual grains (presence of heavy minerals) (Jacobs and Roberts 2007; Roberts et al. 1999) and secondarily on diverse bleaching conditions.

Age estimates and discussion

The age estimates of this study (Table 5) are given with the 1σ uncertainty and after a residual dose of 4 % had been subtracted from the D_e values, except for D_e values of the pIRIR signal at 225 °C of the two young samples as the level of the residual signal at that temperature is usually low. For both pIRIR at 290 and 225 °C, the test dose measurements corrected properly for sensitivity changes, since the average recycling ratio of 95 % of the aliquots was within the accepted 0.9 to 1.10. For the $pIRIR_{290}$ signal, the mean g value was −2.34 ± 0.04 % per decade and mean recuperation was 0.6 %.

In general, feldspar ages are in chronostratigraphic order (Fig. 13) and indicate a late Pleistocene deposition; $pIRIR_{290}$ dating estimations revealed ages of 56.2 ± 4.7 ka for the uppermost aeolianites overlying the beach calcarenite

Table 5 Calculated ages using the appropriate statistical model

Sample	Condition	Model selection Model	Age (ka)
CG-OPS	Aeolian	CAM	56.2 ± 4.7
CG-PS	Beach calcarenite	CAM	59.8 ± 5.1
CG-UP	Shallow marine	CAM	78.4 ± 6.9
CG-01	Aeolian	CAM	61.6 ± 5.6
CG-02	Aeolian	MAM	69.5 ± 8.5
CG-03	Aeolian	CAM	74.4 ± 7.5
AGTS	Aeolian	CAM	66.6 ± 6.1
SD-01	Young aeolian	CAM	1.3 ± 0.03
SD-02	Young aeolian	CAM	1.3 ± 0.1

(59.8 ± 5.1 ka) and shallow marine deposits (78.4 ± 6.9 ka) matching the MIS 3, MIS 4, and possibly the end of MIS 5a which are characterized by a prolonged sea level low transition from a high sea level. For the young aeolianites, the $pIRIR_{225}$ gave an age of 1.3 ± 0.2 ka, providing evidence for sand movement and extensive reworking.

There are a number of different curves for Quaternary sea level changes that could be used for associating the ages derived with the MIS timescales. In this study, we used both Waelbroeck et al. (2002) to compare our dating results with results obtained in other studies using a number of different dating techniques (Fig. 14) and Lambeck's (1996) modeled sea level data which refer to the last interglacial-glacial cycle (Fig. 13).

pIRIR ages obtained for our beach calcarenite and shallow marine samples resulted in age estimates of 59.8 ± 5.1 and 78.4 ± 6.9 ka, respectively. Shallow marine and beach calcarenite deposits present direct evidence of a relatively high sea level at MIS 5 (e.g., Lambeck 1996; Waelbroeck et al. 2002). At one of our sampling points between Ayia Napa and Cape Greco, an exposed stratigraphic column shows that an aeolianite formation (CG-OPS) conformably superimposes the beach calcarenite (CG-PS) which in turn overlies the shallow marine deposits (CG-UP) with pIRIR ages being in stratigraphic order, thus confirming their marine-aeolian association. Our luminescence dating results of the shallow marine sediments (CG-UP) can help provide a rough estimate for the uplift rate of the southeast coastal area Cyprus. An uplift rate of ca. 0.2 mm/year is indicated.

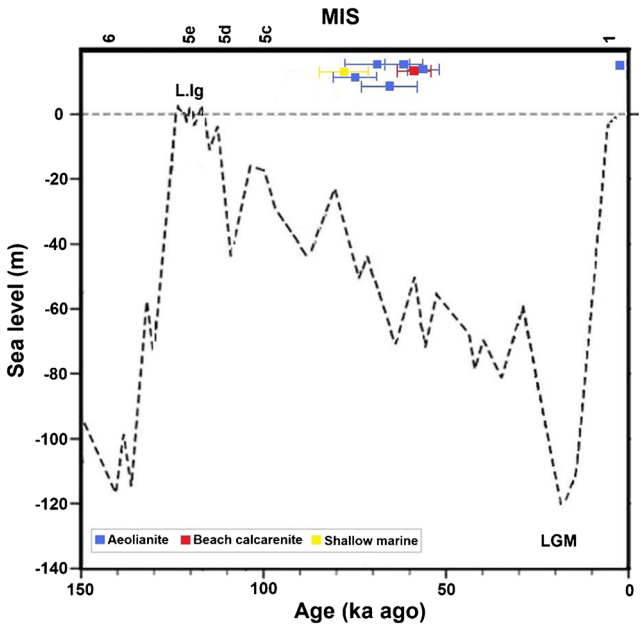

Fig. 13 Comparison of the pIRIR ages of the study area with late Quaternary relative sea level stands of Paros Island located in the central Aegean Sea (after Lambeck 1996). The *graph* shows that deposits are in stratigraphic order with aeolian deposits overlying the littoral (when errors are not considered) except one aeolianite that has an age very close to the dated shallow marine sample. The oldest pIRIR age (CG-UP) obtained from a shallow marine sample underlying a beach calcarenite (CG-PS) and the aeolianites was dated at 78.4 ± 6.9 ka. Based on MIS records (Lambeck 1996), this age suggests the beginning of coastal deposits formation between MISs 5a and 4

Investigation of the factors favoring aeolianite formation has shown that the connection of the aeolianite ridges with the different climatic phases of the Quaternary is not necessarily uniform among different localities (Yallon 1967). For instance, the aeolianites and underlying sediments and soils of the coastal plain of Israel were developed under climatic phases of wet and dry conditions. However, local factors and disturbances were found to be the main driving force for their formation, indicating that the sedimentary cycles of the coastal plain did not necessarily follow the same major cyclic events of the Quaternary (Yallon 1967) which have created distinctive sedimentary coastal formations in other Mediterranean regions. Another instance points out that the local constraints for coastal dunes development exist in the Galilee coastal plain in Israel, where a complete and detailed chronostratigraphic sequence showed that the last glacial period left no sedimentary record (Sivan et al. 1999), as a contrast to many other studies nearby (Netanya and Tel Aviv) (Engelmann et al. 2001; Frechen et al. 2001, 2002; Porat and Wintle 1995; Porat et al. 2004), where aeolian dunes were dated to MIS 3.

It would be expected that the general pattern of our ages should cluster around the last few interglacial episodes, similar to what has been observed elsewhere, further east for example, on the coast of Israel (e.g., Frechen et al. 2004; Mauz et al. 2013) where beachrocks were found to be formed during MIS 5. Indeed, our ages are in fair agreement with these studies but also in a common geochronological framework with the results obtained in studies conducted in southeast coastal Cyprus (e.g., Schellmann and Kelletat 2001) (Fig. 14).

Poole's (1992) ages of 141 ± 4 and 219 ± 16 ka (MISs 6 and 7) as well as Zomeni's (2012) ages of 143 ± 9 and 152 ± 8 ka (MIS 6; Fig. 14 and Table 1), where fauna suitable for uranium-series dating (*Cladocora caespitosa*) was used, indicate that our dated aeolianites (MISs 3, 4, and possibly 5) were deposited in an event later than the littoral deposits of these studies, pointing out that aeolianite formation was most probably initiated at a sea level lower than that of the littoral, just after sea level started falling and the unconsolidated sediments of the last interglacial seafloor were exposed to the dominant winds, favoring their redeposition in the form of sand dunes on the newly exposed shelf. However, there exist an extensive "time lag" between our aeolianite ages and some of the U/Th dating results of other studies in the area (Poole 1992; Zomeni 2012) which is not expected.

Of particular interest to our luminescence studies are two aeolianite OSL age estimates of 60.9 ± 4.4 and 57.9 ± 5.2 ka (Noller 2009), which were found to be in agreement with our dated aeolianites, providing additional evidence for aeolian

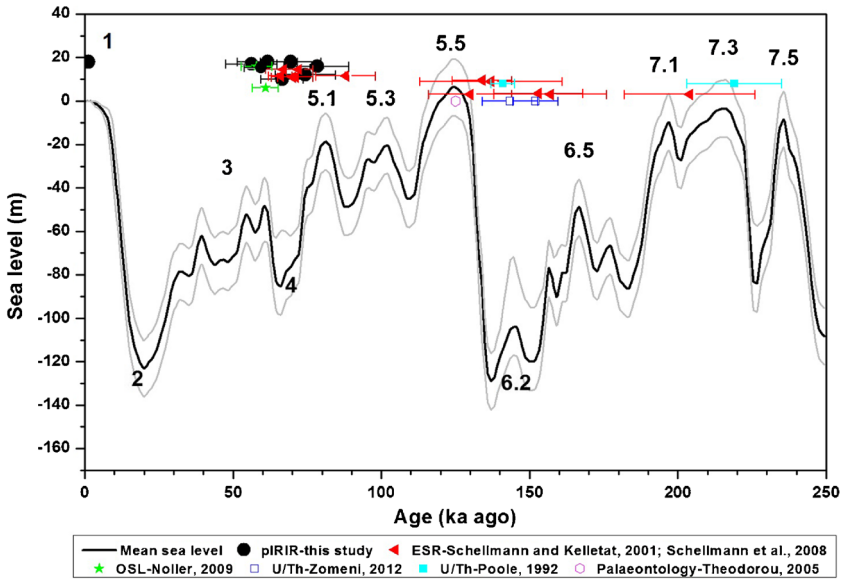

Fig. 14 Comparison of our pIRIR ages with other dating studies conducted in the same area plotted on Waelbroeck et al. (2002) relative sea level stands derived by benthic foraminifer oxygen isotopic ratios from the North Atlantic and equatorial Pacific Ocean. From the *graph*, it is clear that our pIRIR results (*black dots*) represent a later event than that of the U/Th dating on littoral deposits (post-dating the littoral deposits) (Poole 1992; Zomeni 2012)

depositional events in SE Cyprus mainly after the MIS 5a when the sea level started falling.

The deposition of the aeolianites is more commonly associated with a prevailing wind regime. For the aeolianites of our study area, it is believed that west-southwest winds transported the exposed littoral sediments landward. This is supported by the presence of reworked skeletal fragments of marine organisms in our aeolian samples and also by other paleowind studies in the Eastern Mediterranean region. The luminescence-dated (65 ka) aeolianites in the Palestine (kurkar ridges) at the Levant (Frechen et al. 2002) have been interpreted as representing typical dunes formed simultaneously along the coastline by a perpendicular (southwest) to the shoreline wind direction. Field observations in another study from Gaza (Zaineldeen 2010) also showed that cross-beds within the kurkar layers were deposited by a westerly and southwesterly paleowind. The same conclusion regarding wind directions was drawn by Yallon and Laronne (1971) at an aeolianite coastal ridge a few tens of kilometers northern, suggesting a dominant westerly and southwesterly wind regime for the area in the past.

Conclusions

This paper presented a suite of ages for the aeolianites and underlying beach calcarenite and shallow marine deposits found along the coast of Ayia Napa and Cape Greco, in SE coast of Cyprus revealing the occurrence of aeolian activity during MISs 3, 4, and possibly late 5. In general, dune-forming activity ceased along the SE coast of Cyprus at around 60 ka, with dune building commencing about 75 ka most probably under a dominant southwesterly wind regime. A recent reworking and depositional activity of the late Holocene (MIS 1) is also evident.

The comparison of our coastal deposit ages with other absolute dating studies in the area showed that not all the coastal deposits along SE Cyprus were formed at MISs 3, 4, and 5. However, the underlying mechanisms that could explain such variety are not fully understood. A clear case is the U/Th littoral deposits dated at a sea level lowstand at MIS 6 (e.g., Poole 1992; Zomeni 2012).

Our analyses suggest that the pIRIR SAR protocol on feldspars produced reliable equivalent dose values. Performance tests such as preheat plateau, dose recovery, and residual bleaching checks were carried out to confirm the suitability of our SAR protocol. Some variety of the numerical parameters that were observed in D_e value distributions were effectively treated by making use of D_e distribution analysis and selecting the appropriate statistical models which led to accurate and precise D_e values with considerable reduction in associated age errors.

Even though our luminescence dating approach seems to produce reliable results, there exists a source of uncertainty in the calculated ages. The environmental dose rates of the dated deposits have been subject to changes since their initial deposition due to the infiltration of $CaCO_3$ forming the carbonate cement. For the dose rate calculations in this study, cementation was assumed to be instantaneous. Further, the state of (dis)equilibrium was not investigated in this study, and hence, its effect on dose rate has not been accounted for. Thus, it is important ages obtained here to be considered with some caution. Despite that, we believe that even if these parameters had been taken into account, changes in the final ages would have been insignificant, keeping ages in the same paleoenvironmental framework.

This study suggests that luminescence dating offers excellent potential for unraveling the geomorphic history of this

region. For the first time, absolute dating information based on luminescence dating of feldspar of coastal deposits was obtained from a coastal area of southeast Cyprus.

Acknowledgments This research has been supported by the EU project "New Archaeological Research Network for Integrating Approaches to ancient material studies" (NARNIA), from the FP7, Marie Curie Action-ITN by the European Commission under contract number 265010. We are thankful to Dr. Pieter Vermeesch, University College London, for his assistance and information provided in the use of the "*RadialPlotter*" application.

References

Aitken MJ (1985) Thermoluminescence dating. Academic Press, London

Ammerman AJ (2010) The first argonauts: towards the study of the earliest seafaring in the Mediterranean. In: Anderson A, Barrett J, Boyle K (eds) The global origins and development of seafaring. McDonald Institute for Archaeological Research, Cambridge, pp. 81–92

Ammerman AJ, Flourentzos P, McCartney C, Noller J, Sorabji D (2006) Two new early sites on Cyprus. Report of the Department of Antiquities. Department of Antiquities, Cyprus, pp. 1–22

Ammerman AJ, Flourentzos P, Gabrielle R, McCartney C, Noller J, Peloso D, Sorabji D (2008) More on the new early sites on Cyprus. Report of the Department of Antiquities. Department of Antiquities, Cyprus, pp. 1–23

Andreucci S, Clemmensen LB, Murray A, Pascucci V (2010) Middle to late Pleistocene coastal deposits of Alghero, Northwest Sardinia (Italy): chronology and evolution. Quat Int 222:3–16

Angelier J (1979) Neotectionique de l'arc Eggen. These d'etat, Uviversity de Paris, Paris

Arnold LJ, Bailey RM, Tucker GE (2007) Statistical treatment of fluvial dose distributions from southern Colorado arroyo deposits. Quat Geochronol 2:162–167

Arnold LJ, Roberts RF, Galbraith SB, DeLong SB (2009) A revised burial dose estimation procedure for optical dating of young and modern-age sediments. Quat Geochronol 4(4):306–325

Athanassas C, Zacharias N (2010) Recuperated-OSL dating of quartz from Aegean (south Greek) raised Pleistocene marine sediments: current results. Quat Geochronol 5:65–75

Athanassas C, Bassiakos Y, Wagner GA, Timpson ME (2012) Exploring paleogeographic conditions at two Paleolithic sites in Navarino, Southwest Greece, dated by optically stimulated luminescence. Geoarchaeology 27:237–258

Auclair M, Lamothe M, Huot S (2003) Measurement of anomalous fading for feldspar IRSL using SAR. Radiat Meas 37(4–5):487–492

Bagnall PS (1960) The geology and mineral resources of the Pano Lefkara-Larnaca area. Geological Survey Department of Cyprus, Cyprus Memoir No. 5

Bailey RM (2003) Paper I—the use of measurement-time dependent single-aliquot equivalent-dose estimates from quartz in the identification of incomplete signal resetting. Radiat Meas 37(4–5):511–518

Bailey RM, Arnold LJ (2006) Statistical modelling of single grain quartz D_e distributions and an assessment of procedures for estimating burial dose. Quat Sci Rev 25:2475–2502

Bailey RM, Smith BW, Rhodes EJ (1997) Partial bleaching and the decay form characteristics of quartz OSL. Radiat Meas 27(2):123–136

Bailey RM, Singarayer JS, Ward S, Stokes S (2003) Identification of partial resetting using de as a function of illumination time. Radiat Meas 37(4–5):511–518

Balescu S, Dumas B, Gueremy P, Lamothe M, Lhenaff R, Raffy J (1997) Thermoluminescence dating tests of Pleistocene sediments from uplifted shorelines along the southwest coastline of the Calabrian peninsula (southern Italy). Palaeogeogr Palaeocl 130:25–41

Banerjee D, Murray AS, Botter-Jensen L, Lang A (2001) Equivalent dose estimation using a single aliquot of polymineral fine grains. Radiat Meas 33:73–94

Bateman MD, Holmes PJ, Carr AS, Horton BP, Jaiswal MK (2004) Aeolianite and barrier-dune construction during the last two glacial-interglacial cycles from the southern Cape coast, South Africa. Quat Sci Rev 23:1681–1698

Birot P and De Vaumas E (1962) A description of geomorphological sections in Cyprus. The Geological Survey Department of Cyprus, Annual Report 1961, Report chapter, Cyprus, pp 36–38

Boekschoten GJ (1963) Beachrock at Limani, Chersonisos, Crete. Geol Mijnb 41:3–7

Brooke B (2001) The distribution of carbonate eolianites. Earth-Sci Rev 55:135–164

Bulur E, Bøtter-Jensen L, Murray AS (2000) Optically stimulated luminescence from quartz measured using the linear modulation technique. Radiat Meas 32(5–6):407–411

Buylaert J-P, Murray AS, Thomson KJ, Jain M (2009) Testing the potential of an elevated temperature IRSL signal from K-feldspar. Radiat Meas 44:560–565

Buylaert J-P, Thiel C, Murray A, Vandenberghe D, Yi S, Lu H (2011) IRSL and post-IR IRSL residual doses recorded in modern dust samples from the Chinese loess plateau. Geochronometria 38: 432–440

Buylaert J-P, Jain M, Murray AS, Thomsen KJ, Thiel C, Sohbati R (2012) A robust feldspar luminescence dating method for middle and late Pleistocene sediments. Boreas 41:435–451

Choi JH, Murray AS, Cheong CS, Hong DG, Chang HW (2003) The resolution of stratigraphic inconsistency in the luminescence ages of marine terrace sediments from Korea. Quat Sci Rev 22:1201–1206

Dermitzakis MD (1973) The occurrences of Pleistocenic deposits in SE Sitia district (E Crete). Bull Geol Soc Greece 10:180–222

Dermitzakis MD, De Vos J (1986) Evolution and succession of mammal fauna in the Pleistocene environment of island of Crete (in Greek). Ann Géol Pays Hellén 18:407–420

Ducloz C (1964) Notes on the geology of the Kyrenia range. Geological Survey Department of Cyprus, Annual Report for the year 1963, Cyprus, pp 57–66

Ducloz C (1968) Les formations Quaternaires de la region de Klepini (Chypre) et leur place dans la chronologie du Quaternaire Mediterraneen (the Quaternary formations of the region Klepini (Cyprus) and their place in the chronology of the Quaternary Mediterranean). Societe de Physique et d'Histoire Naturelle de Geneve, Geneva, Switzerland, Arch Sci 20(2):123–198

Duller GAT (2008) Single-grain optical dating of Quaternary sediments: why aliquot size matters in luminescence dating. Boreas 37:589–612

El-Asmar HM (1994) Aeolianite sedimentation along the north-western coast of Egypt; evidence for middle to late Quaternary aridity. Quat Sci Rev 13:699–708

El-Asmar HM, Wood P (2000) Quaternary shoreline development: the northwestern coast of Egypt. Quat Sci Rev 19:1137–1149

Elmejdoub N, Mauz B, Jedoui Y (2011) Sea-level and climatic controls on late Pleistocene coastal aeolianites in the Cap Bon peninsula, northeastern Tunisia. Boreas 40:198–207

Engelmann A, Neber A, Frechen M, Boenigk W, Ronen A (2001) Luminescence chronology of Upper Pleistocene and Holocene eolianites from Netanya South—Sharon Coastal Plain, Israel. Quat Sci Rev 20:799–804

Fornós JJ, Clemmensen LB, Gómez-Pujol L, Murray AS (2009) Late Pleistocene carbonate aeolianites on Mallorca, western Mediterranean: a luminescence chronology. Quat Sci Rev 28(25–26):2697–2709

Frechen M, Dermann B, Boenigk W, Ronen A (2001) Luminescence chronology of aeolianites from the section at Givat Olga-coastal plain of Israel. Quat Sci Rev 20:805–809

Frechen M, Neber A, Dermann B, Tsatskin A, Boenigk W, Ronen A (2002) Chronostratigraphy of aeolianites from the Sharon coastal plain of Israel. Quat Int 89:31–44

Frechen M, Neber A, Tsatskin A, Boenigk W, Ronen A (2004) Chronology of Pleistocene sedimentary cycles in the Carmel coastal plain of Israel. Quat Int 121(1):41–52

Galbraith RF, Laslett GM (1993) Statistical models for mixed fission track ages. Nucl Tracks Rad Meas 21(4):459–470

Galbraith RF, Roberts RG (2012) Statistical aspects of equivalent dose and error calculation and display in OSL dating: an overview and some recommendations. Quat Geochronol 11:1–27

Galbraith RF, Roberts RG, Laslett GM, Yoshida H, Olley JM (1999) Optical dating of single and multiple grains of quartz from Jinmium rock shelter, northern Australia: part I, experimental design and statistical models. Archaeometry 41:339–364

Galili E, Sevketoglu M, Salamon A, Zviely D, Mienis HK, Rosen B and Moshkovitz S (2009) Quaternary beach deposits, coastal morphology, tectonics and sea-level changes, on the coast of northern Cyprus, and their possible implications on Neolithic colonization. In: Sagy A, Bookman S, Hamiel Y, Mushkin A, Nahmias Y, Medvedev B and Heimann A (eds) Israel Geological Society (2009), Abstracts, 51

Galili E, Sevketoglu M, Salamon A, Zviely D, Mienis HK, Rosen B and Moshkovitz S (2011) Late Quaternary morphology, beach deposits, sea-level changes, and uplift along the coast of Cyprus and its possible implications on early colonists. In: INQUA 501 Seventh Plenary Meeting and Field trip: Odessa, Ukraine (2011), pp 21–28

Gavish E, Friedman GM (1969) Progressive diagenesis in Quaternary to late tertiary carbonate sediments. J Sediment Petrol 39:980–1006

Godfrey-Smith DI, Huntley DJ, Chen WH (1988) Optical dating studies of quartz and feldspar sediment extracts. Quat Sci Rev 7:373–380

Goy JL, Hillaire-Marcel C, Zazo C, Ghaleb B, Dabrio CJ, González A, Bardají T and Civis J (2003) U-series ages of coral-bearing littoral deposits with *Strombus bubonius* of MIS 7 from La Marina (Alicante, SE Spain). A reappraisal of the Thyrrenian chronostratigraphy in the Mediterranean Sea. In: Mastronuzzi G and Sansò P (eds) Project IGCP 437—coastal environmental change during sea-level highstands: a global synthesis with implication for management of future coastal change, Puglia (2003) final conference. Quaternary coastal morphology and sea-level changes GI^{2}S coast, Research publication, Puglia, 4:109–11.

Guérin G, Mercier N (2012) Preliminary insight into dose deposition processes in sedimentary media on a scale of single grains: Monte Carlo modelling of the effect of water on the gamma dose rate. Radiat Meas 47:541–547

Guérin G, Mercier N, Adamiec G (2011) Dose-rate conversion factors: update. Ancient TL 29:5–8

Hearty PJ, Kindler P (1997) The stratigraphy and surficial geology of new providence and surrounding islands, Bahamas. J Coast Res 13(3): 798–812

Hillaire-Marcel C, Gariepy C, Ghaleb B, Goy JL, Zazo C, Barcelo JC (1996) U-series measurements in Tyrrhenian deposits from Mallorca—further evidence for two last-interglacial high sea levels in the Balearic Islands. Quat Sci Rev 15:53–62

Hogrel MT (1974) Contribution a l' etude de faunes quaternaires merines en Mediterranee orientale (Crete, Karpathos) (Contribution to the study of marine Quaternary fauna in the Eastern Mediterranean (Crete, Karpathos)). PhD Thesis, Universite d'Orleans, France.

Horowitz M (1965) The geology of the Koma tou Yialou—Cape Andreas area (East Karpas Peninsula). Cyprus Geological Survey, Published report, Cyprus

Huntley DJ, Lamothe M (2001) Ubiquity of anomalous fading in K-feldspars and the measurement and correct. Can J Earth Sci 38(7): 1093–1106

Imbrie J, Hays JD, Martinson DG, McIntyre A, Mix AC, Morley JJ, Pisias NG, Prell WL, Shackleton NJ (1984) The orbital theory of Pleistocene climate: support from a revised chronology of the marine δ^{18}O record. In: Berge AL, Imbrie J, Hays J, Kukla G, Saltzman B (eds) Milankovitch and climate, part 1: dreidel. Norwell, Mass, pp. 269–305

Jacobs Z, Roberts RG (2007) Advances in optically stimulated luminescence (OSL) dating of individual grains of quartz from archaeological deposits. Evol Anthropol 16:210–223

Jacobs Z, Duller GAT, Wintle AG (2003) Optical dating of dune sand from Blombos cave, South Africa: II—single grain data. J Hum Evol 44:613–625

Jacobs Z, Dulle GAT, Wintle AG, Henshilwood CS (2006) Extending the chronology of deposits at Blombos cave, South Africa, back to 140 ka using optical dating of single and multiple grains of quartz. J Hum Evol 51:255–273

Jain M, Murray AS, Bøtter-Jensen L (2003) Characterisation of bluelight stimulated luminescence components in different quartz samples: implications for dose measurement. Radiat Meas 37(4–5):441–449

Kelletat D (1979) Geomorphologische studien an den Kusten Kretas (Geomorphological studies on the coasts of Crete). Göttingen, Abhandlungen der Akademie der Wissenschaften 32:1–105 (in Deutsch)

Kendrick GW, Wyrwoll KH, Szabo BJ (1991) Pliocene-Pleistocene coastal events and history along the western margin of Australia. Quat Sci Rev 10:419–439

Kinnaird T (2008) Tectonic and sedimentology response to diachronous continental collision in the easternmost Mediterranean, Cyprus. Ph.D. Thesis, University of Edinburgh, Edinburgh, Scotland

Klappa CF (1980) Rhizoliths in terrestrial carbonates: classification, recognition, genesis and significance. Sedimentology 27:613–629

Klasen N, Fiebig M, Preusser F, Radtke U (2006) Luminescence properties of glaciofluvial sediments from the Bavarian alpine foreland. Radiat Meas 41:866–870

Knapp AB (2010) Cyprus' earliest prehistory: seafarers, foragers and settlers. J World Prehist 23:79–120

Krbetschek MR, Rieser U, Zöller L, Heinicke J (1994) Radioactive disequilibria in palaeodosimetric dating of sediments. Radiat Meas 23: 485–489

Lambeck K (1996) Sea level change and shoreline evolution in Aegean Greece since upper Paleolithic time. Antiquity 70:588–610

Lambeck K, Purcell A (2005) Sea-level change in the Mediterranean Sea since the LGM: model predictions for tectonically stable areas. Quat Sci Rev 24:1969–1988

Lea DW, Martin PA, Pak DK, Spero HJ (2002) Reconstructing a 350 ky history of sea level using planktonic Mg/Ca and oxygen isotope records from a Cocos ridge core. Quat Sci Rev 21:283–293

Lepper K, McKeever SWS (2002) An objective methodology for dose distribution analysis. Radiat Prot Dosim 101:349–352

Li S, Li B (2006) Dose measurement using the fast component of LM-OSL signals from quartz. Radiat Meas 41(5):534–541

Li B, Li S, Wintle AG (2008) Overcoming environmental dose rate changes in luminescence dating of waterlain deposits. Geochronometria 30:33–40

Lowick SE, Trauerstein M, Preusser F (2012) Testing the application of post-IR-IRSL dating to fine grain waterlain sediments. Quat Geochronol 8(1):33–40

Mauz B, Buccheri G, Zoller L, Greco A (1997) Middle to upper Pleistocene morphostructural evolution of the NW-coast of Sicily: thermoluminescence dating and palaeontological-stratigraphical evaluations of littoral deposits. Palaeogeogr Palaeocl 128:269–285

Mauz B, Elmejdoub N, Nathan R, Jedoui Y (2009) Last interglacial coastal environments in the Mediterranean–Saharan transition zone. Palaeogeogr Palaeocl 279:137–146

Mauz B, Fanelli F, Elmejdoub N, Barbieri R (2012) Coastal response to climate change: Mediterranean shorelines during the last interglacial (MIS 5). Quat Sci Rev 54:89–98

Mauz B, Hijma M, Amorosi A, Porat N, Galili E, Bloemendal J (2013) Aeolian beach ridges and their significance for climate and sea level: concept and insight from the Levant coast (East Mediterranean). Earth-Sci Rev 121:31–54

McKeever SWS, Chen R (1997) Luminescence models. Radiat Meas 27: 625–661

McLaren SJ (1995) Early carbonate diagenetic fabrics in the rhizosphere of late Pleistocene aeolian sediments. J Geol Soc 152:173–181

Mercier J, Angelier J, Delibassis N, Gerard P, Kerdiles Y (1974) Les deformations Plio-Quaternaires en extension en Crete meridionale (Ierapetra, Greece) (The Pliocene-Quaternary deformations in southern Crete (Ierapetra, Greece)). Reunion annuelle des Sciences de la Terre: Pont-a-Mousson 285 (in French)

Moseley F (1976) The Neogene and Quaternary of Akrotiri, Cyprus determined by means of a rapid ground reconnaissance assisted by stereo-line-overlap photographs. Mercian Geol 6:49–58

Moshkovitz S (1963) Palaeontological notes. The Geological Survey Department, Annual Report for the year 1962, Report chapter pp 6–8

Mount JF, Cohen AS (1984) Petrology and geochemistry of rhizoliths from Plio-Pleistocene fluvial and marginal lacustrine deposits, East Lake Turkana. J Sediment Petrol 54:263–275

Mourtzas N (1990) Tectonic movements in east coasts of Crete during the Quaternary. PhD thesis, Hellenic National Technical University, Athens, Greece (in Greek)

Moutzas N, Fytrolakis N (1988) Neotectonic movements in Trachoulas Cape in south coasts of Heraklion prefecture of Crete. Bull Geol Soc Greece 20:237–250 (in Greek)

Murray AS, Olley JM (1999) Determining sedimentation rates using luminescence dating. In: Bruns P, Hass HC (eds) Determination of sediment accumulation rates. Trans Tech Publications, Switzerland, GeoResearch Forum, pp. 121–144

Murray AS, Wintle AG (2000) Luminescence dating of quartz using an improved single-aliquot regenerative-dose protocol. Radiat Meas 32:57–73

Murray AS, Wintle AG (2003) The single aliquot regenerative dose protocol: potential for improvements in reliability. Radiat Meas 37: 377–381

Murray-Wallace CV, Belperio AP, Cann JH (1998) Quaternary neotectonism and intra-plate volcanism: the Coorong to Mount Gambier coastal plain, southeastern Australia: a review. In: Vita Finzi C, Stewart C (eds) Coastal tectonics. Geological Society, London, pp. 255–267

Murray-Wallace CV, Bourman RP, Prescott JR, Williams F, Price DM, Belperio AP (2010) Aminostratigraphy and thermoluminescence dating of coastal aeolianites and the later Quaternary history of a failed delta: the river Murray mouth region, South Australia. Quat Geochronol 5:28–49

Nathan P, Mauz B (2008) On the dose-rate estimate of carbonate-rich sediments for trapped charge dating. Radiat Meas 43:14–25

Nielsen KA, Clemmensen LB, Fornos JJ (2004) Middle Pleistocene magnetostratigraphy: data from a carbonate aeolian system, Mallorca, western Mediterranean. Quat Sci Rev 23:1733–1756

Noller J (2009) The geomorphology of Cyprus. Cyprus Geological Survey, Open File Report

Olley JM, Murray A, Roberts RG (1996) The effects of disequilibria in the uranium and thorium decay chains on burial dose rates in fluvial sediments. Quat Sci Rev 15:751–760

Olley J, Caitcheon G, Murray A (1998) The distribution of apparent dose as determined by optically stimulated luminescence in small aliquots of fluvial quartz: implications for dating young sediments. Quat Sci Rev 17:1033–1040

Olley JM, Caitcheon G, Roberts RG (1999) The origin of dose distribution in fluvial sediments, and the prospect of dating single grains from fluvial deposits using optically stimulated luminescence. Radiat Meas 30:207–217

Olley JM, De Deckker P, Roberts RG, Fifield LK, Yoshida H, Hancock G (2004a) Optical dating of deep-sea sediments using single grains of quartz: a comparison with radiocarbon. Sediment Geol 169:175–189

Olley JM, Pietsch T, Roberts RG (2004b) Optical dating of Holocene sediments from a variety of geomorphic settings using single grains of quartz. Geomorphology 60:337–358

Oueslati A (1994) Les côtes de la Tunisie, recherches Sur leur evolution au quaternaire (The coasts of Tunisia, research on their evolution during the quaternary). Publication de la Faculté des Sciences Humaines et Sociales de Tunis 35:402

Pantazis TM (1966a) Tyrrhenian terraces of Larnaka area of southeastern Cyprus. Cyprus Geological Survey Department, annual report for the year (1966), report chapter, pp 29–34

Pantazis TM (1966b) Tyrrhenian deposits of the Karpas peninsula, Cyprus Geological Survey Department, annual report for the year (1966)

Pantazis TM (1966c) Tyrrhenian terraces of Larnaka area of southeastern Cyprus, Cyprus Geological Survey Department, annual report for the year (1966)

Pantazis TM (1967) The geology and mineral resources of the Pharmakas-Kalavasos area. Cyprus Geological Survey Department, Memoir No.8

Pascucci V, Sechi D, Andreucci S (2014) Middle Pleistocene to Holocene coastal evolution of NW Sardinia (Mediterranean Sea, Italy). Quat Int 328:3–20

Paskoff R and Sanlaville P (1983) Les côtes de la Tunisie: variation du niveau marin depuis le Tyrrhénien (The coasts of Tunisia: variation in sea level since the Tyrrhenian). Collection de la maison de l'orient méditerranéen,série géographique et préhistorique 14:189 in French

Paskoff R, Sanlaville P (1986) Oscillations climatiques en Tunisie littorale depuis le dernier interglaciaire jusqu'au début de l'Holocène (Coastal climate oscillations in Tunisia since the last interglacial to the early Holocene). Bulletin de l'Association française pour l'étude du quaternaire 23:78–83 in French

Pavlopoulos K, Karkanas P, Triantaphyllou M, Karyballis E, Tsourou T, Palyvos N (2006) Paleoenvironmental evolution of the coastal plain of Marathon, Greece, during the late Holocene: depositional environment, climate, and sea level changes. J Coast Res 22(2):424–438

Peters JM (1985) Neogene and Quaternary vertical tectonics in the south Hellenic arc and their effect on concurrent sedimentation processes. PhD Thesis, Universiteit van Amsterdam, Amsterdam, The Netherlands

Pirazzoli PA (2005) A review of possible eustatic, isostatic and tectonic contributions in eight late-Holocene relative sea-level histories from the Mediterranean area. Quat Sci Rev 24:1989–2001

Polymeris GS, Erginal AE, Kiyak NG (2012) A comparative morphological, compositional and TL study of Tenedos (Bozcaada) and Şile aeolianites, Turkey. Mediterr Archaeol Ar 12(2):129–132

Poole AJ (1992) Sedimentology, neotectonics and geomorphology related to tectonic uplift and sea-level change: Quaternary of Cyprus. PhD Thesis, University of Edinburgh, Edinburgh, Scotland

Poole AJ, Robertson AHF (1991) Quaternary uplift and sea-level changes at active plate boundary, Cyprus. J Geol Soc 148:909–921

Poole AJ and Robertson AHF (1998) Pleistocene fanglomerate deposition related to uplift of the Troodos ophiolite, Cyprus. In: Robertson AHF, Emeis K., Richter C and Camerlenghi A (eds) Proceedings of the Ocean Drilling Program, Scientific Results 160:545–566

Poole AJ, Robertson AHF, Shimmield G (1990) Late Quaternary uplift of the Troodos ophiolite, Cyprus; uranium-series dating of Pleistocene coral. Geology 18:894–897

Porat N, Wintle AG (1995) IRSL dating of aeolianites from the late Pleistocene kurkar ridge, Israel. INQUA XIV, Berlin

Porat N, Wintle AG, Ritte M (2004) Mode and timing of kurkar and hamra formation, Central Coastal Plain, Israel. Isr J Earth Sci 53: 13–25

Prescott JR, Hutton JT (1988) Cosmic ray and gamma ray dosimetry for TL and ESR. International Journal of Radiation Applications and Instrumentation. Part D. Nucl Tracks Radiat Meas 14:223–227

Prescott JR, Hutton JT (1994) Cosmic ray contribution to dose rates for luminescence and ESR dating: large depths and long-term time variations. Radiat Meas 23(2–3):497–500

Prescott JR, Stephan LG (1982) The contribution of cosmic radiation to the environmental dose for thermoluminescence dating, latitude, altitude and depth dependencies. J Eur Stud Group Phys Chem Math Tech Appl Archaeol 6:17–25

Preusser F, Degering D, Fuchs M, Hilgers A, Kadereit A, Klasen N, Krbetschek M, Richte D, Spencer JQG (2008) Luminescence dating: basics, methods and applications. J Quat Sci 57:95–149

Price DM, Brooke BP, Woodroffe CD (2001) Thermoluminescence dating of aeolianites from Lord Howe Island and south-west Western Australia. Quat Sci Rev 20:841–846

Psarianos P (1961) Tyrrhenian deposits of South Crete. Ann Géol Pays Hellén 12:12–17 (in Greek)

Rittenour TM, Goble RJ, Blum MD (2005) Development of an OSL chronology for late Pleistocene channel belts in the lower Mississippi valley. Quat Sci Rev 24:2539–2554

Roberts HM, Wintle AG (2001) Equivalent dose determination for polymineral fine-grains using the SAR protocol: application to a Holocene sequence of the Chinese loess plateau. Quat Sci Rev 20: 859–863

Roberts RG, Galbraith RF, Olley JM, Yoshida H, Laslett GM (1999) Optical dating of single and multiple grains of quartz from Jinmium rock shelter, northern Australia: part II, results and implications. Archaeometry 41:365–395

Roberts RG, Galbraith RF, Yoshida H, Laslett GM, Olley JM (2000) Distinguishing dose populations in sediment mixtures: a test of single-grain optical dating procedures using mixtures of laboratory dosed quartz. Radiat Meas 32:459–465

Rodnight H, Duller GAT, Wintle AG, Tooth S (2006) Assessing the reproducibility and accuracy of optical dating of fluvial deposits. Quat Geochronol 1:109–120

Roesch WC, Attix FH (1968) Basic concepts of dosimetry. In: Attix FH, Roesch WC (eds) Radiation dosimetry, volume I: fundamentals. Academic Press, New York and London

Roskosch J, Tsukamoto S, Meinsen J, Frechen M, Winsemann J (2012) Luminescence dating of an upper Pleistocene alluvial fan and aeolian sandsheet complex: the Senne in the Münsterland embayment, NW Germany. Quat Geochronol 10:94–101

Schatz A, Buylaert J-P, Murray A, Stevens T, Scholten T (2012) Establishing a luminescence chronology for a palaeosol-loess profile at Tokaj (Hungary): a comparison of quartz OSL and polymineral IRSL signals. Quat Geochronol 10:68–74

Schellmann G, Kelletat D (2001) Chronostratigraphische Untersuchungen litoraler und äolischer Formen und Ablagerungen an der Südküste von Zypern mittels ESR Altersbestimmungen an Molluscen-und Landschneckenschalen (Chronostratigraphic studies of littoral and aeolian forms and deposits on the southern coast of Cyprus by ESR age determinations on Molluscen and land snail shells). Essener Geographische Arbeiten 32:75–98 (in Deutsch)

Schellmann G, Beerten K, Radtke U (2008) Electron spin resonance (ESR) dating of Quaternary materials. Quat Sci J (Eiszeitalter und Gegenwart) 57:150–178

Schmidt ED, Murray AS, Sirocko F, Tsukamoto S, Frechen M (2011) IRSL signals from Maar Lake sediments stimulated at various temperatures. E&G Quat Sci J 60:105–115

Shackleton NJ (1987) Oxygen isotopes, ice volume and sea level. Quat Sci Rev 6:183–190

Shackleton NJ, Backman J, Zimmerman H, Kent DV, Hall MA (1984) Oxygen isotope calibration of the onset of ice rafting and history of glaciation in the North Atlantic region. Nature 307:620–623

Shen Z, Mauz B (2009) D_e determination of quartz samples showing falling D_e (t) plots. Radiat Meas 44:566–570

Sivan D, Porat N (2004) Evidence from luminescence for late Pleistocene formation of calcareous aeolianite (kurkar) and palaeosol (hamra) in the Carmel coast, Israel. Palaeogeogr Palaeocl 211:95–106

Sivan D, Gvirtzman G, Sass E (1999) Quaternary stratigraphy and paleogeography of the Galilee Coastal Plain, Israel. Qual Res 51:280–294

Spooner NA (1994) The anomalous fading of infra-red stimulated luminescence from feldspars. Radiat Meas 2:625–632

Steffen D, Preusser F, Schlunegger F (2009) OSL quartz age underestimation due to unstable signal components. Quat Geochronol 4(5): 353–362

Stevens T, Markovic SB, Zech M, Hambach U, Sümegi P (2011) Dust deposition and climate in the Carpathian Basin over an independently dated last glacial-interglacial cycle. Quat Sci Rev 30:662–681

Stokes S, Bray HE, Blum MD (2001) Optical resetting in large drainage basins: tests of zeroing assumptions using single-aliquot procedures. Quat Sci Rev 20:879–885

Symeonides N (1967) Pleistocene sequences in south-east Crete and the nearby islands of Chrisi, Strogilo, Koufonisi. Ann Géol Pays Hellén 18:407–420 in Greek

Theodorou G (2005) Paleontological study of Cyprus. Special report of the University of Athens in Greek

Thiel C, Coltorti M, Tsukamoto S, Frechen M (2010) Geochronology for some key sites along the coast of Sardinia (Italy). Quat Int 222:36–47

Thiel C, Buylaert JP, Murray AS, Terhorst B, Hofer I, Tsukamoto S, Frechen M (2011a) Luminescence dating of the Stratzing loess profile (Austria)—testing the potential of an elevated temperature post-IR IRSL protocol. Quat Int 234(1–2):23–31

Thiel C, Terhorst B, Jaburová I, Buylaert JP, Murray AS, Fladerer FA, Damm B, Frechen M, Ottner F (2011b) Sedimentation and erosion processes in middle to late Pleistocene sequences exposed in the brickyard of Langenlois/Lower Austria. Geomorphology 135(3–4):295–307

Thiel C, Buylaert J-P, Murray AS, Elmejdoub N, Jedoui Y (2012) A comparison of TT-OSL and post-IR IRSL dating of coastal deposits on Cap Bon peninsula, north-eastern Tunisia. Quat Geochronol 10: 209–217

Thomsen KJ, Jain M, Bøtter-Jensen L, Murray AS, Jungner H (2003) Variation with depth of dose distributions in single grains of quartz extracted from an irradiated concrete block. Radiat Meas 37:315–321

Thomsen KJ, Murray AS, Jain M, Bøtter-Jensen L (2008) Laboratory fading rates of various luminescence signals from feldspar-rich sediment extracts. Radiat Meas 43:1474–1486

Thomsen KJ, Murray AS, Jain M (2011) Stability of IRSL signals from sedimentary K-feldspar samples. Geochronometria 38:1–13

Tsakalos E, Christodoulakis J, Charalambous L (2015) The dose rate calculator (DRc)—a Java application for dose rate and age determination based on luminescence and ESR dating. Archaeometry. doi: 10.1111/arcm.12162

Tsiolakis E and Zomeni Z (2008) Geological map of the Pafos–Kallepeia area, sheets 16 III and IV, scale 1:25,000. Cyprus Geological Survey

Turner WM (1971a) Geology of the Polis-Kathikas area, Cyprus. PhD Thesis, University of New Mexico, Albuquerque, NM, United States

Turner WM (1971b) Quaternary sea levels of western Cyprus. Quaternaria 15:197–202

Vacher HL, Hearty PJ and Rowe MP (1995) Stratigraphy of Bermuda: nomenclature, concepts, and status of multiple systems of classification. In: Curran HA and White B (eds) Terrestrial and shallow marine geology of the Bahamas and Bermuda. Geological Society of America Special Paper 300, Geological Society of America, Boulder: CO, pp 271–294

Vasiliniuc Ş, Vandenberghe DAG, Timar-Gabor A, Panaiotu C, Cosma C, van den Haute P (2012) Testing the potential of elevated temperature post-IR IRSL signals for dating Romanian loess. Quat Geochronol 10:75–80

Vouvalidis KG, Syrides GE and Albanakis KS (2005) Holocene morphology of the Thessaloniki Bay: impact of sea level rise. Zeitschrift fur Geomorphologie

Waelbroeck C, Labeyrie L, Michel E, Duplessy JC, McManus JF, Lambeck K, Balbon E, Labracherie M (2002) Sea-level and deep water temperature changes derived from benthic foraminifera isotopic records. Quat Sci Rev 21:295–305

Wintle AG (1973) Anomalous fading of thermoluminescence in mineral samples. Nature 245(5421):143–144

Woodroffe CD, Murray-Wallace CV, Bryan EA, Brooke BP, Price DM, Heijnis H (1995) Late Quaternary sea-level highstands from the Tasman Sea: evidence from Lord Howe Island. Mar Geol 125:61–72

Yallon DH (1967) Factors affecting the lithification of eolianite and interpretation of its environmental significance in the coastal plain of Israel. J Sediment Petrol 37:1189–1199

Yallon DH, Laronne J (1971) Internal structures in aeolianites and palaeowinds, Mediterranean coast, Israel. J Sediment Petrol 41: 1059–1064

Zaineldeen U (2010) Palaeowind estimation of cross-bedding within the aeolian kurkar layers of the Gaza formation, Gaza strip, Palestine. Geol Croat 63(1):55–65

Zomeni Z (2012) Quaternary marine terraces on Cyprus: constraints on uplift and pedogenesis, and the geoarchaeology of Palaipafos. PhD Thesis, Oregon State University, Oregon, United States